CHALMERS

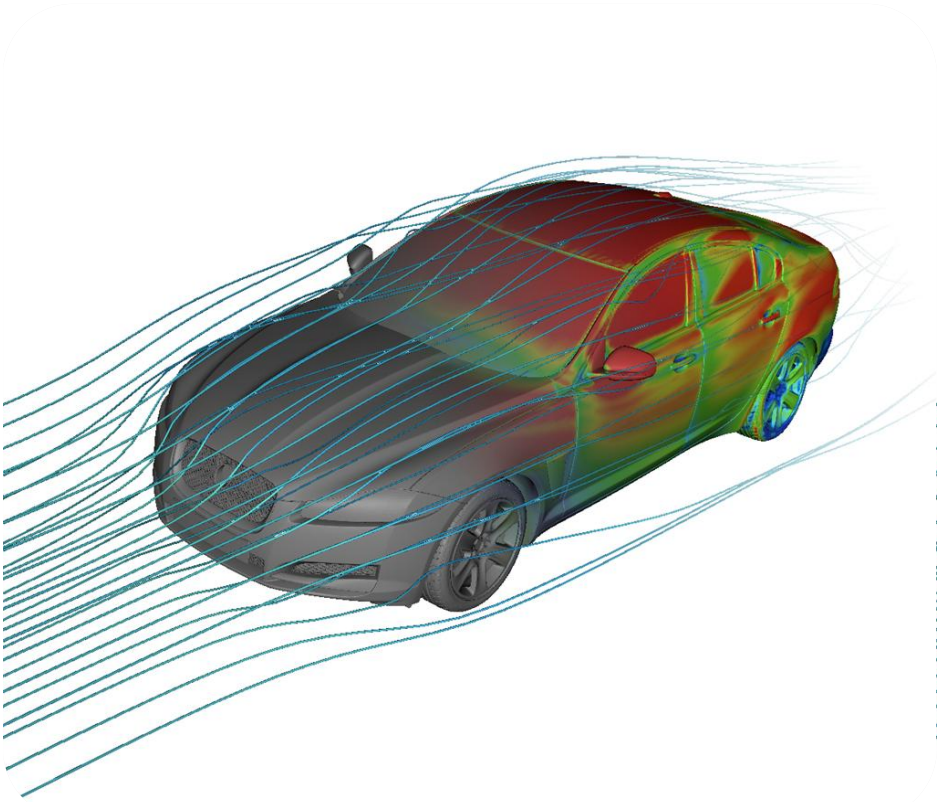

A Computational Investigation of Wheel and Underbody Flow Interaction

Investigating the Relationship between Aerodynamic Forces, Ground Simulation and Wheel Rotation for a Saloon and an Estate Car

Master's Thesis in the Automotive Engineering Master's Programme

SOFIE KOITRAND

SVEN REHNBERG

Department of Applied Mechanics
Division of Vehicle Engineering & Autonomous Systems
Road Vehicle Aerodynamics
CHALMERS UNIVERSITY OF TECHNOLOGY
Göteborg, Sweden 2013
Master's thesis 2013:24

MASTER'S THESIS IN AUTOMOTIVE ENGINEERING

A Computational Investigation of Wheel and Underbody Flow

Investigating the Relationship between Aerodynamic Forces, Ground Simulation and Wheel Rotation for a Saloon and an Estate Car

SOFIE KOITRAND

SVEN REHNBERG

Department of Applied Mechanics
Division of Vehicle Engineering & Autonomous Systems
Road Vehicle Aerodynamics
CHALMERS UNIVERSITY OF TECHNOLOGY

Göteborg, Sweden 2013

A Computational Investigation of Wheel and Underbody Flow Interaction

Investigating the Relationship between Aerodynamic Forces, Ground Simulation and Wheel Rotation for a Saloon and an Estate Car

SOFIE KOITRAND

SVEN REHNBERG

Master's Thesis 2013:24
ISSN 1652-8557
Department of Applied Mechanics
Division of Vehicle Engineering & Autonomous Systems
Road Vehicle Aerodynamics
Chalmers University of Technology
SE-412 96 Göteborg
Sweden
Telephone: + 46 (0)31-772 1000

Cover:
The Jaguar XF Saloon with streamlines

Chalmers Reproservice
Göteborg, Sweden 2013

A Computational Investigation of Wheel and Underbody Flow Interaction
Investigating the Relationship between Aerodynamic Forces, Ground Simulation and Wheel Rotation for a Saloon and an Estate Car
Master's Thesis in the *Automotive Engineering Masters Programme*
SOFIE KOITRAND
SVEN REHNBERG
Department of Applied Mechanics
Division of Vehicle Engineering & Autonomous Systems
Road Vehicle Aerodynamics
Chalmers University of Technology

ABSTRACT

The use of moving ground and rotating wheels (MVG&RW) when testing road vehicles in wind tunnels have previously been shown to largely affect the results, however it is still not the standard test prodecure for many manufacturers. This also means that simulations are set up to match the static behaviour of the experimetal tests. However, when most companies today turn their efforts to the underbody of the vehicle in an effort to improve aerodynamics, stationary conditions are no longer adequate.
This report aims at investigating how the rotation of the front and rear wheels in combination of moving ground influence the local, as well as the global, flow fields and especially the wake behind the vehicle, by the use of Computational Fluid Dynamics (CFD). Two different vehicle models based on the same platform, namely the Jaguar XF Saloon and Sportbrake, are used to set up eight different cases for each vehicle. The research has been set up to enable comparison with earlier experimental research. The results are divided into three groups giving the results due to the addition of a moving ground, rotating front wheels and rotating rear wheels. By adding a moving ground the drag and front lift increase noticeably, whereas the rear lift decreases significantly. The addition of front wheel rotation has little effect on the global results, whereas the addition of rear wheel rotation largely decreases both the drag and the rear lift. By adding these three groups up largely the same results are achieved as when comparing the fully stationary cases to the cases with MVG&RW conditions, namely that the addition of MVG&RW conditions noticeable reduces the drag and the rear lift, whereas front lift hardly changes.

Key words:

External Aerodynamics, Road Vehicle Aerodynamics, CFD, Rotating Wheels, Moving Ground, Lattice Boltzmann, Transient Flow

Contents

Preface

We would like to thank our supervisor Adrian Gaylard for the immense support and advice provided throughout this project. Further, we would like to thank *Jaguar Land Rover* for enabling this project and for providing us with models, support and computers. Especially we would like to thank the *Aerodynamics department at JLR* and all JLR emploees who have helped us out in different ways.

Further, we would like to thank our examiner Professor Lennart Löfdahl for his recommendations and support, without which this project would never have happened. Also, a special thanks to Ph.D. student Lisa Larsson for her genuine interest and great help during our years as Master's students.

We would finally like to thank our families and friends for their support during our time at *Chalmers University of Technology.*

Göteborg May 2013

Sofie Koitrand and Sven Rehnberg

Nomenclature

C_D	Coefficient of drag
C_{Dl}	Coefficient of local drag
C_L	Coefficient of lift
C_{LF}	Coefficient of front lift
C_{LR}	Coefficient of rear lift
C_p	Coefficient of pressure
$C_{p_{tot}}$	Coefficient of total pressure

CAD	Computer Aided Design
CFD	Computational Fluid Dynamics
LBM	Lattice Boltzmann Method
LBE	Lattice Boltzmann Equation
NS	Navier-Stokes
RANS	Reynolds Averaged Navier-Stokes
MRF	Multiple Reference Frame
VR	Variable Resolution
MVG	Moving Ground
RW	Rotating Wheels
RWF	Rotating Wheels Front
RWR	Rotating Wheels Rear
JLR	Jaguar Land Rover
LDV	Laser Doppler Velocimetry

1 Introduction

Adequate simulation of moving ground and rotating wheels when investigating the aerodynamic behaviour of road vehicles has in previous research been claimed to be of significant importance, especially in terms of underbody aerodynamics (Elofsson & Bannister, 2002). This report outlines a numerical investigation of the influence of MVG&RW (Moving Ground and Rotating Wheels) on a Saloon and an Estate model of the same platform and manufacturer, namely the Jaguar XF.

1.1 Background

Wind tunnels have been used in the automotive industry since the 1940's (VanGordon & Walter, 2008) as a means to quantify the forces acting on the vehicle body, due to the relative motion between the vehicle and the air, mainly in the longitudinal and vertical directions. For a long time the standard way of doing this has been to simply place the vehicle in the wind tunnel and control the relative air motion to achieve the required simulated vehicle speed. This method provides, in general, good results, especially if deficiencies such as wind tunnel blockages are taken into account. There are however some areas where this method produces less satisfactory results, e.g. a correct simulation of underbody aerodynamics (Cogotti, 1995). This is an area which has not been the subject of as extensive focus as the upper body area, and the fact that this area has been somewhat overlooked in the past means that a greater focus on the underbody design might lead to relatively large improvements in overall performance in terms of aerodynamics.

Research has shown (Elofsson & Bannister, 2002) that by simulating rotating wheels and moving ground in wind tunnels, and thus changing the boundary layer conditions in the underbody area, not only better estimations of integral forces, i.e. drag and lift, can be achieved but also a more accurate simulation of local flow fields, e.g. around the wheel arches. This is important in order to understand and estimate local forces, but also to understand how design changes in one area of the vehicle can affect the flow field in other areas.

The computational resources available today means that correlation between numerical CFD (Computational Fluid Dynamics) simulations and wind tunnel testing is, in general, good (Landström, Löfdahl, & Walker, 2009). CFD simulations have the advantage of being relatively quick and inexpensive which allows for many concepts and changes to be evaluated without the need for a physical model. Expensive and time consuming wind tunnel tests can thus be reduced to "end of design programme" evaluation and correlation. The main advantage of CFD simulation is the ability to investigate different flow field attributes, e.g. pressure and velocity, on a detailed level throughout the entire flow field. This means greater ability to understand complex flow behaviours and interaction.

1.2 Objectives

The study described in this report aims to investigate the influence of moving ground and rotating wheels on the external aerodynamics, on the Saloon and Sportbrake models of the Jaguar XF passenger car. This is done using CFD simulations and focuses on wheel wake behaviour and the influence of rotating wheels on global flow field and on the base wake structure. The work is mainly based on, and can be seen as a comparative study of, the work done by P. Elofsson and M. Bannister (Elofsson & Bannister, 2002) and G. Wickern and N. Lindener (Wickern & Lindener, 2000).

1.3 Scope

To reach the objectives the research is performed by simulating different combination of wheel rotation with and without moving ground simulation in CFD.

Apart from the obvious differences in geometry, care has been taken to ensure that the models are as identical as possible in terms of underbody geometry, wheel design, etc. This has been done for the sake of better comparability when investigating the simulation results. The models feature detailed engine compartments, realistic cooling flow, realistic wheels with scanned tyre surfaces and standard production underbody, for more accurate simulations which can be compared to previous wind tunnel research. For simulations with stationary wheels the tyres used are scanned with a deformed contact patch equivalent to that seen on passenger cars.

The research does not investigate the aerodynamic performance of the models, but merely the influence of MVG&RW; hence the data will be presented in delta values. Raw data with company specific values will be presented in appendices that will not be published due to rights. The research is also limited to numerical evaluation; no physical wind tunnel work has been performed. All comparative mentioning of wind tunnel results will be taken from already published research, and will therefore be of different car models than described in this report. It should consequently be noted that discrepant findings from different reports may depend on the use of different car models, as well as the use of different wind tunnels. This might also be true when it comes to other CFD research, if different algorithms, turbulence models, etc. have been used.

2 Literature Review

The area of investigation has been commented on by several authors such as (Elofsson & Bannister, 2002), (Wickern & Lindener, 2000), (Wickern, Zwicker, & Pfadenhauer, 1997), (Landström, Löfdahl, & Walker, 2009) and (Wäschle, 2007), who agrees on a decrease in total drag due to MVG&RW conditions compared to stationary conditions. All but Wickern et al. also discuss and are in agreement that the most significant factor contributing to the decrease of total drag is the interference effect of the rear wheel and wheel housing wakes with the base wake.

Several studies have also been performed to validate the ability of CFD codes to predict aerodynamic forces, with good results, such as (Landström, Löfdahl, & Walker, 2009), (Wäschle, 2007), (Wäschle, Cyr, Kuthada, & Wiedemann, 2004), (Duncan D, Fischer, & Kandasamy, 2010), (Boujo, et al., 2008), (Kandasamy, et al., 2012) and (Fischer, Kuthada, Mercker, Wiedemann, & Duncan, 2010).

2.1 Review of effect of MVG&RW

(Wickern, Zwicker, & Pfadenhauer, 1997) found that as much as 25 % of the total drag during MVG&RW conditions can be attributed to the wheel and wheel housings, which leads to the conclusion that simulating rotating wheels need to be given the same priority as moving ground simulations.

(Wickern & Lindener, 2000) performed experimental tests in the Audi wind tunnel on a sportscar and the results can be found in Table 2-1. It was found that a moving ground together with boundary layer removal increased drag and decreased rear lift compared to a stationary setup. It was also found that rotating wheels lowered drag and increased lift, especially front lift. The drag reduction is said to depend mostly on the changes in the airflow at the rear end of the vehicle whereas the lift changes depend mostly on changes at the front. The lift effect is thought to depend on a lesser through-flow and an improved underbody flow due to rotating wheels. Finally it was discovered that with only rotating rear wheels both the front and rear lift decrease, whereas if only the front ones rotate there is a need to overcome the air build up in front of the rear wheels leading to an increase in lift.

(Elofsson & Bannister, 2002) performed experimental tests at the Pininfarina Wind Tunnel on a generic version of a Volvo Sedan and a Volvo Squareback. The results can be found in Table 2-1 together with the results by Wickern and Lindener. It was found that the interference effects of the rear wheel and wheel housing wakes with the base wake posed the main reason for the drag reduction due to MVG&RW. It was also found that this effect was more significant with a Sedan than with a Squareback, which is said to depend on an improved flow balance around the base wake region. As with Wickern and Lindener it was found that adding a moving ground increased drag and front lift slightly and decreased rear lift. The contribution to the decrease in rear lift was thought to be the increased mass flow travelling underneath the vehicle underbody. By only adding rotating front wheels there was a small increase in drag, although the local drag decrease 450 mm behind the front wheel was significant. This discrepancy between local drag and total drag was attributed to the smaller wake from the rotating front wheels hitting the rear wheels and thereby allowing the rear wheel wake to grow and increase its interference with the base wake, and hence increasing drag. A large drag decrease followed the addition of rotating rear wheels. It was found that without rotating rear wheels there is a strong outflow of the rear wheel housings

resulting in a wide wake, and that there is a large wake region directly behind the lower part of the rear wheel contributing to drag; neither of which was seen with rotating wheels.

Table 2-1 Summary of experimental results presented by Elofsson & Bannister and Wickern & Lindener

Effect due to	Study	Wind Tunnel	Car	ΔC_D	ΔC_{LF}	ΔC_{LR}	Conditions
MVG	Elofsson & Bannister	Pininfarina	Volvo Generic Sedan	+0.006	+0.003	-0.009	
MVG	Elofsson & Bannister	Pininfarina	Volvo Generic Sqrback	+0.004	+0.001	-0.011	
MVG	Wickern & Li ndener	Audi WT	Sportscar	+0.008	-0.005	-0.010	
RWF	Elofsson & Bannister	Pininfarina	Volvo Generic Sedan	-0.002	+0.017	+0.002	MVG
RWF	Elofsson & Bannister	Pininfarina	Volvo Generic Sqrback	+0.002	+0.014	-0.009	MVG
RWF	Wickern & Li ndener	Audi WT	Sportscar	0.000	+0.022	+0.006	MVG
RWF	Wickern & Li ndener	Audi WT	Sportscar	-0.002	+0.018	+0.009	MVG&RWR
RWR	Elofsson & Bannister	Pininfarina	Volvo Generic Sedan	-0.019	-0.004	+0.002	MVG&RWF
RWR	Elofsson & Bannister	Pininfarina	Volvo Generic Sqrback	-0.008	-0.005	-0.019	MVG&RWF
RWR	Wickern & Li ndener	Audi WT	Sportscar	-0.020	-0.009	-0.002	MVG&RWF
RWR	Wickern & Li ndener	Audi WT	Sportscar	-0.018	-0.005	-0.005	MVG

(Landström, Löfdahl, & Walker, 2009) also found a decrease in global drag with MVG&RW compared to stationary conditions. CFD comparisons were performed with the MRF (Multiple Reference Frame) method to simulate rotating wheels and without fully transient simulations, and the achieved results comfirmed the experimental results, however with some discrepensies.

(Wäschle, 2007) found that the interference effects between the underbody flow and the rear wheel wakes contributed the most to the changes in drag and lift with

MVG&RW and, in accordance with others, a decrease in total drag with MVG&RW compared to stationary conditions.

All conclude that MVG&RW ought to be incorporated in aerodynamic testing and simulation of road vehicles, due to its large influence on the flow structure and the overall drag.

2.2 Review of CFD correlation

All papers are based on wind tunnel experiments, however (Landström, Löfdahl, & Walker, 2009) and (Wäschle, 2007) also performed CFD analysis to compare their results, which has been shown to correlate well. The correlation between CFD analysis and experimental results considering rotating wheels has also been investigated by (Wäschle, Cyr, Kuthada, & Wiedemann, 2004), with good results. The report compares one steady state solver (Star-CD) and one transient solver (PowerFLOW) with experimental wind tunnel data.

Further, (Duncan D, Fischer, & Kandasamy, 2010), (Kandasamy, et al., 2012), (Boujo, et al., 2008) and (Fischer, Kuthada, Mercker, Wiedemann, & Duncan, 2010) have evaluated the prediction of the Lattice Boltzmann based CFD software Exa PowerFLOW, with promising results for both drag and lift.

(Duncan D, Fischer, & Kandasamy, 2010) performed wind tunnel and CFD investigations on four different vehicle models and compared the result. The results were found to correlate well and trends for moving ground effects were very well predicted. Front and rear lift values from the CFD simulations showed a trend toward higher lift values than the experimental values, however still close to perfect correlation.

(Kandasamy, et al., 2012) show a good correlation between CFD results and experimental results with a maximum of 2% difference in the drag coefficient, and a maximum of 15 counts difference in the lift coefficients with a sliding mesh setup to simulate the rotating wheels. When using MRF or a rotating wall boundary condition to simulate rotating wheels they instead have a 5% maximum error of the drag coefficient. The lift values of the rotating wall show an error of up to 27 counts, whereas those of the MRF correlates well with the sliding mesh with values differing up to 13 counts.

(Fischer, Kuthada, Mercker, Wiedemann, & Duncan, 2010) investigated a notchback and a SUV model in an open jet wind tunnel and compared with CFD results. For the notchback the drag coefficient differs a few counts, whereas the total lift coefficient is about 20 counts higher for the CFD simulation for each setup. The front lift coefficient is between 6 and 7 counts higher for each setup whereas the rear lift coefficient is consistently about 15 counts higher for the CFD results with a CAD model compared to the wind tunnel results.

(Boujo, et al., 2008) show an indication of an absolute difference in the lift coefficient C_L of ± 10 counts comparing CFD results to experimental results.

3 Theory

To understand aerodynamics it is important to understand the interaction between fluids and bodies, boundary layer theory, and relations such as the Bernoulli equation. Since the use of CFD is essential in this research, also the theory behind the chosen CFD software, Exa PowerFLOW, is of importance.

3.1 Fundamental aerodynamics

The basic theory behind aerodynamics is pressure differences, which can be described and applied with the Bernoulli equation. By the use of pressure the drag and lift forces can be calculated. For a more complete investigation of the flow, which is required if CFD is to be satisfactory, the Navier-Stokes equations are used.

3.1.1 The Bernoulli equation

Investigations of road vehicle aerodynamics are mainly based on the Bernoulli equation (Equation 1) (Barnard, 2009), which for road vehicles can be simplified to Equation 2 assuming steady incompressible flow (White, 2009). The Bernoulli equation gives the relation between the pressure and the velocity of the flow, and hence the pressure distribution where the first term represents the static pressure and the second the dynamic pressure. Given that the Bernoulli equation is valid along a streamline it follows that Equation 3 must be valid, where P_∞ denotes the free stream pressure, and v_∞ the free stream velocity. From this, the dimensionless pressure coefficient C_p can be derived according to Equation 4 (McBeath, 2011). The pressure coefficient is more convenient to investigate than pressure since it only depends on speed. By looking at Equation 4 it can be noted that C_p will reach its highest value (1) at the stagnation point, and that a C_p of zero indicates that the local velocity is equal to the free stream velocity. It can also be noted that a negative pressure coefficient is possible whenever the local velocity is higher than that of the free stream.

$$\int_1^2 \frac{\partial V}{\partial t} ds + \int_1^2 \frac{\partial p}{\rho} + \frac{1}{2}(v_2^2 - v_1^2) + g(z_2 - z_1) = 0 \qquad \textit{Equation 1}$$

$$P_{static} + \frac{1}{2}\rho v^2 = Constant \qquad \textit{Equation 2}$$

$$P_\infty + \frac{1}{2}\rho v_\infty^2 = P + \frac{1}{2}\rho v^2 \qquad \textit{Equation 3}$$

$$C_p = \frac{P - P_\infty}{\frac{1}{2}\rho v_\infty^2} = 1 - \frac{\frac{1}{2}\rho v^2}{\frac{1}{2}\rho v_\infty^2} = 1 - \frac{v^2}{v_\infty^2} \qquad \textit{Equation 4}$$

Since pressure equals force over a given area, C_p can be used to calculate the forces acting on the body according to Equation 5. Since road vehicle aerodynamics mainly concerns drag and lift forces, the equation can be rewritten as Equation 6 and

Equation 7 where C_D for drag and C_L for lift are used instead of C_p. These are called drag and lift factors, and they are dimensionless coefficients describing how the overall shape of the body influences the flow around it (McBeath, 2011).

$$Force = C_p \frac{1}{2} \rho v^2 A \qquad \textit{Equation 5}$$

$$Drag\ force = C_D \frac{1}{2} \rho v^2 A \qquad \textit{Equation 6}$$

$$Lift\ force = C_L \frac{1}{2} \rho v^2 A \qquad \textit{Equation 7}$$

The coefficient of drag can be used to compute the drag in a single point in space, or local drag. By using the momentum and continuity equations it can be shown that;

$$C_D A = \int_{A_p} (1 - C_{p_{tot}}) dA_p - \int_{A_p} \left(1 - \frac{v_x}{v_\infty}\right)^2 dA_p + \int_{A_p} \left(\frac{v_y}{v_\infty}\right)^2 dA_p + \int_{A_p} \left(\frac{v_z}{v_\infty}\right)^2 dA_p \qquad \textit{Equation 8}$$

where $C_{p_{tot}}$ is the coefficient of total pressure and A_p is the area of the measurement plane (Cogotti, 1989). Given values for the different parameters in any point in space Equation 8 can be re-written to give the coefficient of local drag C_{D_l}.

The Bernoulli equation is only a simplified way of explaining the behaviour of a fluid. It is assumed that the total energy of the flow is constant along a streamline, meaning that losses are not accounted for. The sum of the terms on either side of the equal sign in Equation 3 is called the *total pressure* and can be expressed as a pressure coefficient, in a similar manner as the coefficient of pressure, according to Equation 9;

$$C_{p_{tot}} = \frac{P_{t,local} - P_\infty}{\frac{1}{2} \rho v_\infty^2} \qquad \textit{Equation 9}$$

where $P_{t,local}$ is the local total pressure (right hand side in Equation 3). In areas where there are no losses, e.g. in the free stream $P_{t,local} - P_\infty = \frac{1}{2} \rho v_\infty^2$ which means $C_{p_{tot}} = 1$. If however losses are taken into account the local total pressure will not always be constant and $C_{p_{tot}}$ will be less than one. The coefficient of total pressure is thus an effective way of investigating areas of losses, e.g. due to viscous effects. (Issa, 1995) also shows that in viscous flow $C_{p_{tot}}$ can be higher than one by claiming that a local increase can occur as a result of a decrease of total pressure elsewhere in the flow as mechanical energy is redistributed due to viscous stresses.

3.1.2 Navier-Stokes equations

To explain the correct and complete behaviour of a fluid, the energy equation, the continuity equation and the momentum equations, the latter usually called the *Navier-Stokes equations* (Equation 10), are used and take into account e.g. losses and density changes due to high speed flows.

$$\rho g_x = \frac{\partial p}{\partial x} + \mu\left(\frac{\partial^2 u}{\partial u^2} + \frac{\partial^2 u}{\partial y^2} + \frac{\partial^2 u}{\partial z^2}\right) = \rho\frac{du}{dt}$$
$$\rho g_y = \frac{\partial p}{\partial y} + \mu\left(\frac{\partial^2 v}{\partial u^2} + \frac{\partial^2 v}{\partial y^2} + \frac{\partial^2 v}{\partial z^2}\right) = \rho\frac{dv}{dt} \qquad \textit{Equation 10}$$
$$\rho g_z = \frac{\partial p}{\partial z} + \mu\left(\frac{\partial^2 w}{\partial u^2} + \frac{\partial^2 w}{\partial y^2} + \frac{\partial^2 w}{\partial z^2}\right) = \rho\frac{dw}{dt}$$

The Navier-Stokes equations, together with the energy and continuity equations, are the basis for CFD software, even though they are notoriously difficult to solve numerically. Usually simplifications are made, e.g. the flow can be assumed to be incompressible (density is constant) which makes the energy equations redundant and the equations are often time-averaged to obtain a less complex steady-state solution. If the viscosity term is neglected, the *Euler's equations* are obtained (Barnard, 2009) and from this the Bernoulli equation can be derived. This is why the Bernoulli equation does not account for viscous losses.

3.1.3 Vortices

In terms of aerodynamics there is no universally accepted definition of a vortex (Chakraborty, Balachandar, & Adrian, 2005), but it refers to the rotation of fluid particles. The investigation of vortex structures in the automotive industry is important, since the creation of vortices requires energy, and hence increases the drag. Any body that creates lift does so by creating a pressure difference between the upper and lower part of the body. This pressure difference causes air to flow from the high pressure area to the low pressure area and this motion combined with the forward motion of the body creates trailing vortices. Vortices are often unsteady and e.g. the interaction between the side mirror vortex and the greenhouse on a passenger car is a main source of aerodynamic noise. One way of visualising vortices is to identify regions of the flow where the second invariant of the velocity tensor is positive using Equation 11.

$$Q = -\frac{1}{2}\left(\frac{\partial u}{\partial x}\frac{\partial u}{\partial x} + \frac{\partial v}{\partial y}\frac{\partial v}{\partial y} + \frac{\partial w}{\partial z}\frac{\partial w}{\partial z} + 2\frac{\partial u}{\partial y}\frac{\partial v}{\partial x} + 2\frac{\partial u}{\partial z}\frac{\partial w}{\partial x} + 2\frac{\partial v}{\partial z}\frac{\partial w}{\partial y}\right) \qquad \textit{Equation 11}$$

3.1.4 Boundary layer theory

Since there is a relative motion between the air and the floor in a wind tunnel, a boundary layer is developed on the floor. This is a primary source for errors in wind

tunnel testing, since the test object will be partially submersed in the boundary layer (Barnard, 2009). The use of a so called moving ground system, often a belt system combined with a scoop and/or some suction technique, can prevent the relative motion between the air and the floor, and thereby create a more road-like environment. Often the moving ground system is separate from the rotating wheel system, which is achieved with separate belts for each wheel, or rollers. The rotation gives rise to an interference effect with the flow around the wheels, changing the wheel and wheelhousing wake structure and thereby the overall flow structure around the vehicle.

3.2 Computational Fluid Dynamics

Computational Fluid Dynamics, or CFD, is an approximate computer based method used to investigate the behaviour of a fluid and its interactions with a test object, in this case a vehicle. By discretising the governing equations in space and time over a control volume and thereby approximately solving them a solution to the posed problem is achieved. How correct the obtained solution is, in comparison to reality, depends on several factors such as geometry representation, turbulence modelling, mesh quality, available computer capacity, experience etc. In terms of aerodynamic forces CFD is generally more correct in prediction of drag than in prediction of lift. This is due to the fact that even small simulation errors in pressure can result in large deviation in lift, since lift is the results of pressure acting on large surfaces (Kandasamy, et al., 2012).

3.2.1 The Lattice Boltzmann Method

The conventional way of using CFD, the finite volume method, uses the governing equations of the flow, the Navier-Stokes equations, as a starting point. These equations are continuous in space and time and have to be discretised over a control volume in order to be numerically solved. The Lattice Boltzmann method (LBM) relies on particle distribution in time and space, where the discretisation occurs at a microscopic level (Bahram, 2008). This particle distribution can be described by the number of particles with a certain velocity at a certain location in space and time, and is defined as Equation 12;

$$n = f(\vec{c}, \vec{x}, t) \qquad \textit{Equation 12}$$

where n is the number of particles or particle distribution, $\vec{x}$ is the position in space, $\vec{c}$ is a certain speed and t is a certain discrete time step or position in time. The particle distribution is used to determine every relevant fluid parameter, such as density (Equation 13), momentum (Equation 14) and energy (Equation 15);

$$\rho(\vec{x},t) = \int n(\vec{x},\vec{c},t)d\vec{c} \qquad \textit{Equation 13}$$

$$\rho(\vec{x},t)u(\vec{x},t) = \int n(\vec{x},\vec{c},t)\vec{c}d\vec{c} \qquad \textit{Equation 14}$$

$$D\rho(\vec{x},t)T(\vec{x},t) = \int n(\vec{x},\vec{c},t)(\vec{c}-\vec{u})^2 d\vec{c} \qquad \textit{Equation 15}$$

The governing equation in the LBM is the Boltzmann equation (Equation 16) which defines the rate of change of the velocity distribution function n, and can be described as;

$$n(\vec{x}+\vec{c}\Delta t, t+\Delta t) = n(\vec{x},t) + C(n(\vec{x},t)) \qquad \textit{Equation 16}$$

where $C(n(\vec{x},t))$ is the *collision operator*, which describes the transfer of mass, momentum and energy between particles as they move from one cell to another with velocity $\vec{c}$ during the time step Δt and collide, and it must by necessity satisfy the conservation laws. The fact that the discretisation occurs at a microscopic scale and the particle distribution is time and space dependent means that the LBM is inherently transient.

3.2.2 Relation between RANS and LBM

There are several ways of deriving the (macroscopic) Navier-Stokes equations from the Boltzmann equation, which shows why the LBM and the finite volume method can be used to solve the same problems (Chen & Doolen, 1998), (Wagner, 2008).

Since the Lattice Boltzmann equations are already in discrete form, there is no need for further discretisation, as it is with the finite volume method. This minimises the approximation in the solution since the discrete approximation of the LBM occurs at a lower level. LBM solves the pressure locally whereas finite volume method CFD codes have to solve the Poisson equation globally to obtain the pressure. Finite volume methods usually rely on time-averaging (e.g. the Reynolds-Averaged Navier-Stokes (RANS) method) to simplify the governing equations and reduce the computational time. This leaves the simulations steady, whereas LMB simulations are transient. Often, however, it is the time-averaged values that are interesting in aerodynamic investigations. It is therefore necessary to time-average the LMB simulations to obtain the mean values for e.g. drag and lift. The transient data is however still valuable if further understanding of the flow behaviour in areas of highly transient flow is required.

3.2.3 Exa PowerFLOW

In the Lattice Boltzmann based Exa PowerFLOW the CFD simulation is performed in three stages. After importing a surface mesh PowerFLOW automatically generate the grid. Following the grid generation is an automatic decomposition for parallel processing that enables a fairly quick time accurate simulation.

3.2.3.1 Meshing

All CFD codes solve the governing equations (either LBE or NSE) at nodes given by a generated mesh. This necessitates that the geometries of the vehicle and the wind tunnel are represented by a surface mesh that is fine enough to capture geometry changes, and that the volume mesh inside the wind tunnel representing the simulation volume is fine enough in areas where large gradients are expected, such as in wake regions. Usually a coarser volume mesh is created far away from the test object in the virtual wind tunnel with refinement zones closer to the test object. This limits the number of cells and hence minimise the computational capacity needed to solve the calculations.

Meshing in PowerFLOW differentiates from many other CFD codes, since it is performed automatically by the software before the solver starts. Given that the surface representation mesh of the aforementioned geometries is fine enough to capture the surfaces, the software will re-mesh the surface mesh to a computational surface mesh represented by surfels and build a volume mesh according to given parameters such as VR (Variable Resolution) regions. The large difference between PowerFLOW and other codes is that in PowerFLOW the volume mesh (the lattice) grows until it intersects with the facets (elements describing the geometry of the test object), and thereafter builds the surfels, which represents the computational surface mesh. The implication of this is that the resolution of the lattice is independent of the surface representation.

3.2.3.2 Grid refinement strategy

The grid is refined by so called Variable Resolution (VR) regions. Every new VR region splits the cell by the power of two; hence each new level is half the size of the former level (Fares, 2006). VR regions can either be defined by boxes which can be used to create refinement zones within the wind tunnel or by offsets from actual parts which can be used around the test object. A VR region defined by a box and a VR region defined by an offset can be seen in Figure 3-1 where a body fit of VR6 (green) and a simulation volume of VR5 (yellow) is shown. It is possible to set the minimum VR thickness, which is the lowest number of cells allowed in between two VR regions. If this requirement is not achieved by the user, PowerFLOW will ensure it during the discretisation. The higher the number of the VR region, the smaller the size of the mesh is. Normally VR0 is set as part of the wind tunnel and VR10 is set in fine regions such as the grille (VR10 = 1.25 mm).

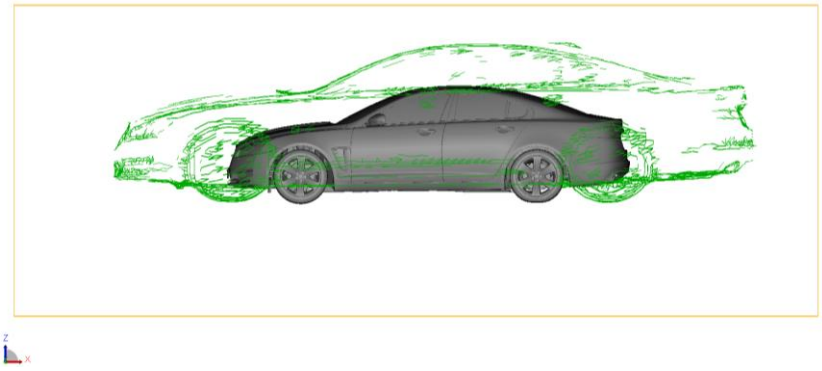

Figure 3-1 VR6 (body fit) and VR5 (simulation volume of wind tunnel)

3.2.3.3 Boundary conditions for rotating parts

To simulate rotating parts of the vehicle, such as fans and wheels, either a rotating wall boundary condition or a local rotating reference frame can be used (Exa Corporation, 2012). A rotating wall boundary condition ensures that the surfels of the rotating part have a given angular velocity around a rotational axis. A local rotating reference frame can be set up with either a MRF (Multiple Reference Frame) region or with a sliding mesh region. With the sliding mesh the mesh changes position and everything inside the defined local rotating reference frame with the definition of sliding mesh is moving (Exa Corporation, 2012). Normally the sliding mesh is used for more complex simulations focusing on how the wheel design influence the aerodynamics whereas the MRF method is used in more general research.

3.2.3.4 Convergence

As is common when using CFD simulations a simulation is considered converged when the difference between iterations is small enough. "Small enough" is not an absolute value and may vary depending on the application. The convergence criterion for transient simulations posses additional difficulties, since the results from a simulation can be unsteady and still be considered converged. This is especially true for bluff body applications, where unsteady vortices can shed from the body but in a consistent fashion. Despite the unsteady nature of these simulations the time average is consistent. One way to deal with this is to continuously record the average values of the forces acting on the body. Once the average values are consistent over a given time period the simulation can be considered to have converged.

The inherit unsteadiness of bluff bodies can cause transient simulations to be very time consuming. The initial fluid parameter values given to each node must be given time to adjust and converge to the given situation, and the presence of unsteady regions of the flow prolongs this process. If care can be taken with the initial values, the simulation time can be reduced and one way of doing this is to use the result from previous simulations as starting values, which is called *seeding* from a previous simulation.

4 Methodology

The models have been prepared in BETA CAE Systems S.A. ANSA 13.2.2, the cases have been prepared in Exa PowerCASE 4.4c and the simulations have been performed with Exa PowerFLOW 4.4c. For post-processing another software by Exa, PowerVIZ 4.4c, has been used.

4.1 Model preparation

Already existing and complete surface meshes of the two cars were provided by JLR, which included all necessary parts. These surface meshes are based on CAD models, and as mentioned in section 1.3 they are detailed in the relevant areas in order to ensure realistic simulations. In general, areas of the surface mesh that are exposed to high speed flow, e.g. the upper body and rear view mirrors, are meshed with higher resolution than areas that experience low speed flow, e.g. engine components and parts of the suspension.

To prepare the simulation cases certain changes to the geometry were necessary, mainly in regards to the suspension and the wheels. For all cases the correct camber and toe values had to be changed, to correspond with standard JLR values. No change was made to the CAD models, but to the surface meshes which were altered using ANSA.

4.1.1 Stationary vs. rotating wheels

In cases where rotating wheels were simulated a gap of a few millimetres was necessary between the wheels and the suspension to ensure that the MRF region used to enclose the rotating part does not intersect with the suspension. Only the spokes of the wheels were enclosed by a MRF region (Figure 4-1). When simulating rotating wheels the rest of the wheels and tyres, as well as the brake discs, were assigned as rotating walls. Since this requires axisymmetric parts, and the scanned tyres feature a deformed contact patch, the tyres models needed modification. The lateral profile of the scanned tyre was revolved around the wheel centre in order to create an axisymmetric tyre (Figure 4-2) which still resembles the original scanning (Figure 4-3). In order to simulate the effect of a deformed contact patch the axisymmetric tyres were allowed to intersect the ground plane with a few millimetres. For a more in-depth study on axisymmetric versus scanned tyres see Appendix B *Tyre Study on XF Saloon* Case 4.

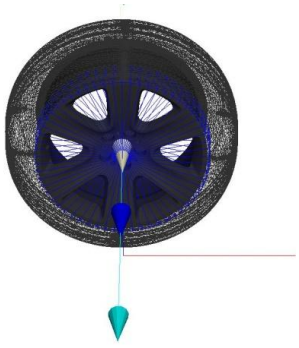

Figure 4-1 Wheel with MRF region enclosing the spokes

Figure 4-2 Axisymmetric Tyre

Figure 4-3 Scanned Tyre

4.2 Case setup

The different cases were prepared in PowerCASE 4.4c according to a by JLR provided standard, with some differing case specific parameters.

4.2.1 Case explanation

Since the objective has been to investigate the influence of rotating wheels and moving ground numerically and compare the results with previous wind tunnel research, the different cases have been, to a large extent, based on the work done by (Elofsson & Bannister, 2002). The configurations of the different cases can be found in Table 4-1.

Table 4-1 Description of cases

Case	Abbreviation	Description
1	Stationary	Baseline case; stationary wheels and ground
2	MVG&RW	Moving ground and rotating wheels
3	MVG&RWF	Moving ground and rotating front wheels, stationary rear wheels
4	MVG&RWR	Moving ground and rotating rear wheels, stationary front wheels
5	RWF	Rotating front wheels, stationary rear wheels and stationary ground
6	RWR	Rotating rear wheels, stationary front wheels and stationary ground
7	RW	Rotating wheels, stationary ground
8	MVG	Moving ground, stationary wheels

The case description for all cases apply for both car models, in order to compare the results from numerical simulations and wind tunnel research, as well as any potential differences between the XF Saloon and the XF Sportbrake.

4.2.2 Case settings

To ensure that the lattice (volume mesh) is fine enough to guarantee a satisfying result several different regions of mesh refinement have been used. The different VR regions are explained in Table 4-2.

Table 4-2 Explanation of VR regions

VR Region	Voxel size	Description
10	1.25 mm	Grill Front valance panel
9	2.5 mm	Front end Front valance panel Lower part of wheels A pillars Front header Cowl Rear end C pillars (Saloon) D pillars (Sportbrake) Intersection between roof and rear window (Saloon) Roof spoiler (Sportbrake) Various rear underbody components
8	5 mm	Entire car (enclosing the VR9 regions)
7	10 mm	Entire car (enclosing the VR8 regions)
6	20 mm	Entire car (enclosing the VR7 regions)
5	40 mm	Boxes enclosing VR6 regions and ground in front of car
4	80 mm	Box enclosing VR5 regions
3	160 mm	Box enclosing VR4 region
2	320 mm	Box enclosing VR3 region
1	640 mm	Box enclosing VR2 region
0	1280 mm	Entire simulation volume

For the cases where rotating wheels are simulated the entire wheels are enclosed in the VR9 region.

In all cases the car models have the same ride height and pitch, and all simulations are of zero yaw situations. The ambient pressure and temperature is set to atmospheric pressure and 20 °C respectively, and the simulated wind speed is 28.1 m/s.

In order to simulate the honeycomb screen used to straightening the flow in the MIRA wind tunnel near Nuneaton in the UK, a suction point is introduced in the virtual wind tunnel 13.5 metres in front of the car (measured from the centre of the wheelbase). The honeycomb screen is also used to break up the floor boundary layer and in the virtual wind tunnel the suction point specifies where floor friction will be turned on. The suction point is turned off when moving ground is simulated. It is then replaced with a 50 metres by 50 metres wide "moving belt" which is simulated using a sliding wall boundary condition. Other important boundary conditions are the use of a velocity inlet, a static pressure outlet and frictionless wall conditions on the tunnel walls and ceiling.

4.2.3 Wheel rotation

To simulate rotating wheels the MRF (Multiple Reference Frame) method was used, as described in section 3.2.3.3 and section 4.1.1. For an in-depth study on the MRF method versus the Sliding mesh method see Appendix A *Sliding mesh vs. MRF (Case 2*).

4.3 Analysis of results

There are a number of ways to visualise and investigate the results from CFD simulations. Parameters of interest, such as total pressure, static pressure and velocity magnitude, can be visualised on the vehicle surface or slicing planes can be used to investigate the behaviour of the flow field in the space around the vehicle. Streamlines and isosurfaces are other examples of visualisation techniques that can be used depending on the purpose of the investigation.

4.3.1 Investigation planes

As mentioned in section 1.1 one of the main advantages of CFD simulations is that the entire flow field can be investigated in detail. This is practically impossible in a wind tunnel and introducing measurement probes to the flow field in a wind tunnel will always, however minimal, alter the flow. LDV (Laser Doppler Velocimetry) can be used without altering the flow but is a very time consuming method.

In order to investigate the results of the simulations described in this report, and to compare it to previous research, several different planes were used and can be seen in Figure 4-4. Plane B1, used by (Elofsson & Bannister, 2002), is placed 450 mm behind the front wheel centres and is used to visualise the local drag, as described by (Cogotti, 1989).

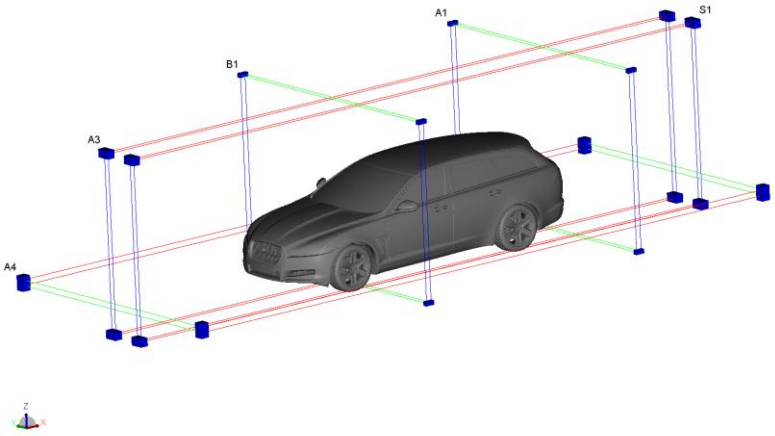

Figure 4-4 Cutting planes used for the post-processing

The investigation in this report that is not a direct comparison with previous research used several other planes. A1 is placed 100 mm behind the rear bumper of the vehicle, while A3 is an xz-plane placed in the centre of the vehicle. A4 is a xy-plane placed 321 (wheel centre) mm above the ground plane in the wheel centres. S1 is, like plane A3, an xz-plane but placed -550 mm from the A3 plane in the y direction.

4.3.2 Standard deviation

A seldom used but useful method to identify areas of unsteady flow is to investigate where the flow has high values of standard deviation of certain parameters. In areas where the flow is steady, such as over the bonnet or over the roof, the standard deviation of for example pressure can be assumed to be small or non-existent. The highly unsteady base wake, by contrast, can be expected to have high values of standard deviation.

Even though all flows are transient (time dependent) in nature they might still be considered steady, meaning that the behaviour of the flow does not change significantly over time. One example would be the flow around a cylinder. The flow separation on the back of the cylinder will not be stationary, but will fluctuate with a certain frequency depending on the free flow velocity. This kind of unsteady wake is called *Kármán vortex street*, and even if the flow is unsteady the average forces acting on the cylinder are constant.

4.3.3 Isosurfaces

Isosurfaces are, as the name suggests, surfaces or equal value of some parameter, and can be thought of as three-dimensional contour lines. In CFD post-processing, isosurfaces are commonly used to encapsulate areas of the flow with parameter values equal, lower or higher than a specific value of interest. For example, as mentioned in section 3.1.1, $C_{p_{tot}}$ values equal or lower to 0 indicates large viscous losses, and thus isosurfaces showing areas of $C_{p_{tot}}$ values equal or lower than 0 are very useful. Figure 4-5 shows such $C_{p_{tot}}$ isosurfaces for the XF Sportbrake for Case 1. Other examples are Figure 5-9, showing Q values equal or higher than 3000 and Figure 5-33 showing pressure standard deviation values equal or higher than 0.075.

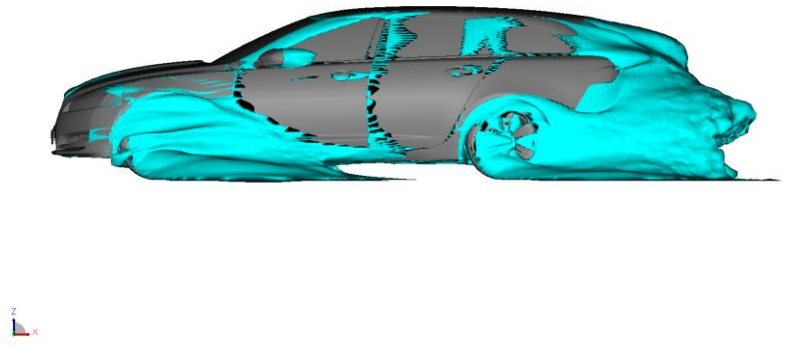

Figure 4-5.Isosurfaces of $C_{p_{tot}}$ equal to or lower than 0 for XF Sportbrake Case 1

5 Results

In this chapter the results will be presented. First the total difference between the stationary and the MVG&RW cases will be presented, followed by the effect induced only by the moving ground, rotation of the front wheels, and rotation of the rear wheels. Finally the effect of unsteadiness upon the results will be presented.

5.1 Stationary vs. moving ground and rotating wheels

The difference between the MVG&RW cases and the stationary cases for both vehicles are presented as delta values in Table 5-1 and in Figure 5-1

Table 5-1 Comparison between Stationary and MVG&RW cases

Notes	ΔC_D	ΔC_{LF}	ΔC_{LR}
JAGUAR XF SALOON			
MVG&RW – Stationary	-0.008	-0.001	-0.055
JAGUAR XF SPORTBRAKE			
MVG&RW - Stationary	-0.009	-0.003	-0.084

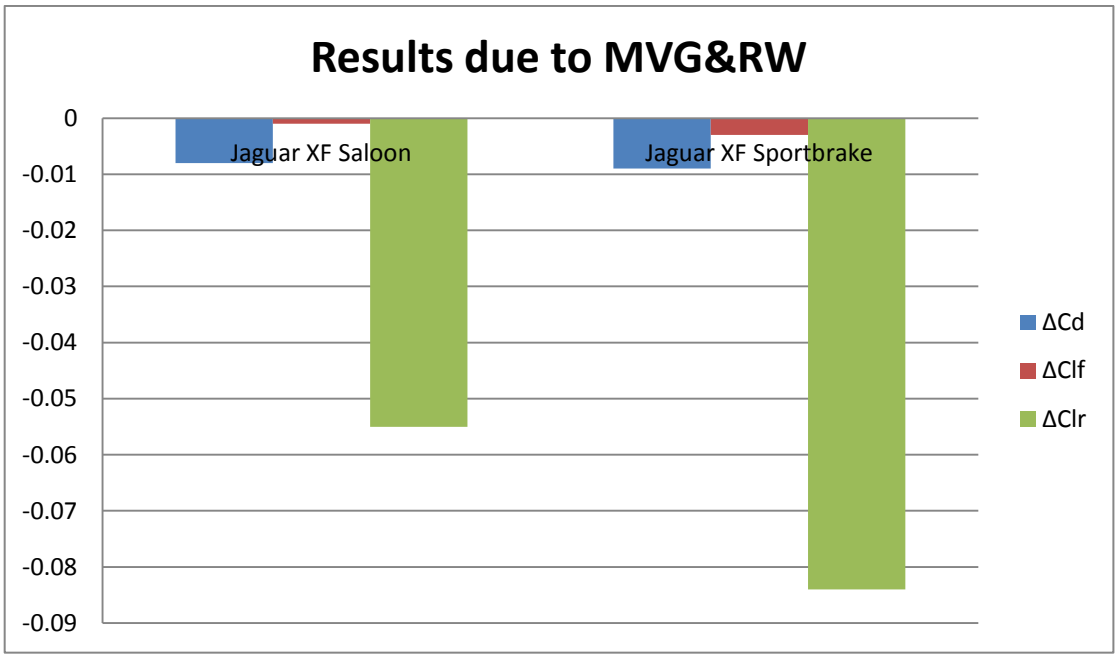

Figure 5-1 Comparison between Stationary and MVG&RW cases

Table 5-1 and Figure 5-1 show the change in C_d, C_{LF} and C_{LR} between Case 1, with stationary wheels and ground, and Case 2 with MVG&RW. The drag reduction on

both car models are close to the typical reduction values of between ten and 20 counts seen from wind tunnel research (Elofsson & Bannister, 2002). The general trend for the two models are the same, with a noticable reduction in drag, a minimal reduction in front lift and a significant reduction in rear wheel lift.

Friction drag on the floor in front and under the car can be seen in Figure 5-3, showing local drag for the XF Saloon Case 1, briefly disturbed by the negative drag propagating from the stagnation point on the front end of the car. This cannot be seen in Figure 5-2, representing Case 2. The local drag on the underside of the car is mostly caused by viscous losses as a result of the turbulence introduced to the flow by the complex and unsmooth underbody. The skin friction drag on the car can also be seen on the bonnet, front screen and roof.

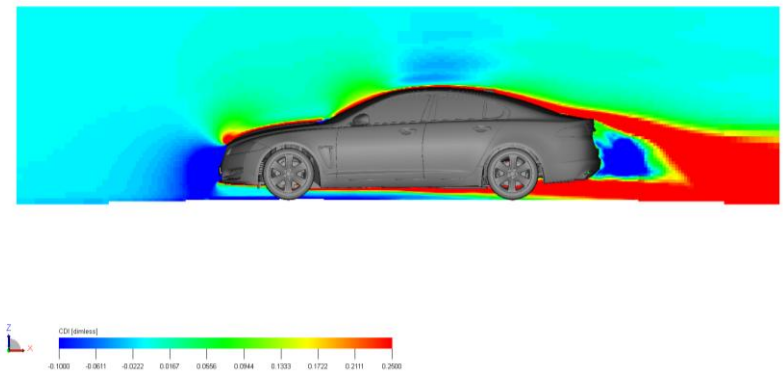

Figure 5-2 Local drag as seen on plane A3 for XF Saloon Case 2 - With MVG&RW

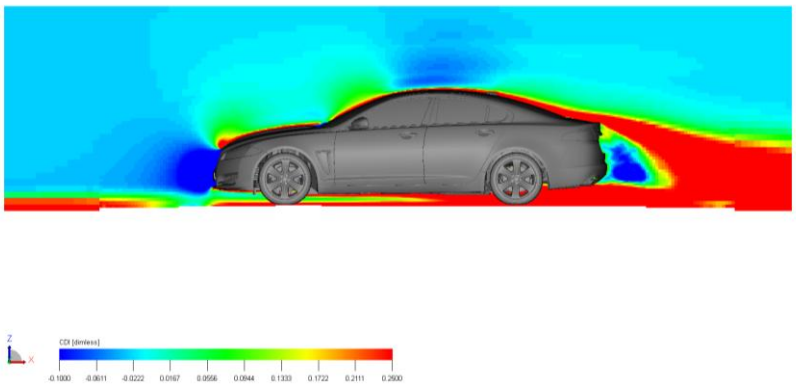

Figure 5-3 Local drag as seen on plane A3 for XF Saloon Case 1 – Stationary

One of the most obvious differences when applying MVG&RW conditions to the virtual wind tunnel is the absence of a boundary layer on the floor. This can clearly be seen in Figure 5-2 where no skin friction drag can be seen in the front. The boundary layer building up on the car is still present. Figure 5-2 also show that no boundary layer exists on the floor under the car, meaning that the lower parts of the wheels will not be submersed in a boundary layer, which is the case in Case 1.

The formation of the boundary layers in Case 1 can also be seen in Figure 5-5 where the floor boundary layer can be seen across the cross section. This cannot be seen in the case of MVG&RW, Figure 5-4.

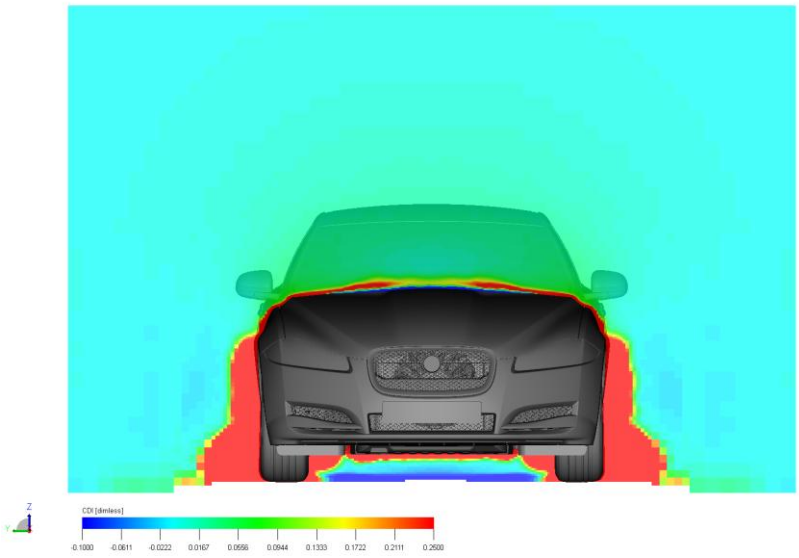

Figure 5-4 Local drag as seen on plane B1 for XF Saloon Case 2 - With MVG&RW

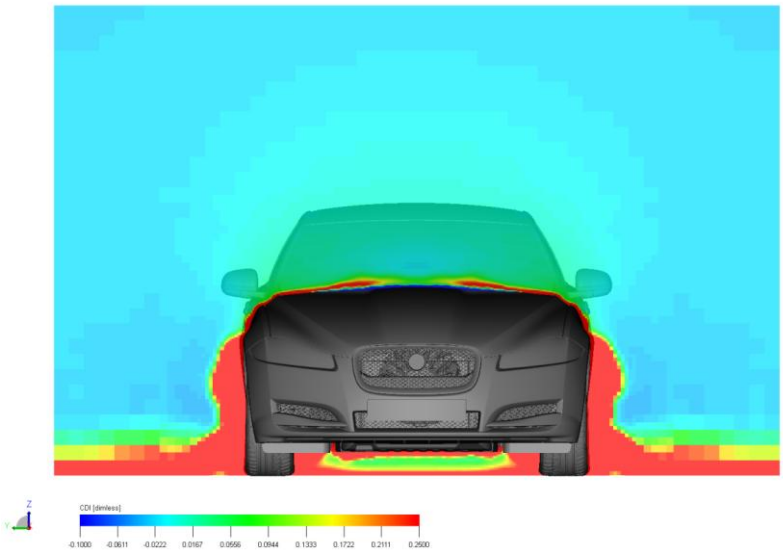

Figure 5-5 Local drag as seen on plane B1 for XF Saloon Case 1 – Stationary

It is also obvious from the figures that it is not only the skin friction and the immediate proximity of the car that causes drag. The wake structures caused by the front wheels are clearly visible as a source of drag, which can be seen in Figure 5-7 showing areas of $C_{p_{tot}}$ less than 0, indicating areas of large losses. By comparing Figure 5-4 and Figure 5-6 of Case 2 and Figure 5-5 and Figure 5-7 of Case 1 it can be seen that, apart from the absence of a floor boundary layer, the wake from the front wheel has changed slightly but the combined wake from the rear wheel and behind the car has changed significantly. The rear wake is aslo affected by the wheel rotation and moving ground, as seen in Figure 5-6, which shows a smaller base wake compared to Figure 5-7.

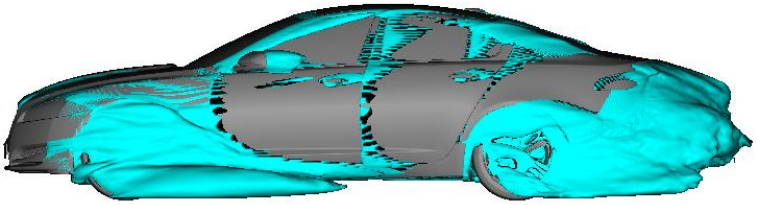

Figure 5-6 Isosurface representing $C_{p_{tot}}$ values equal to or lower than 0 for XF Saloon Case 2 – With MVG&RW

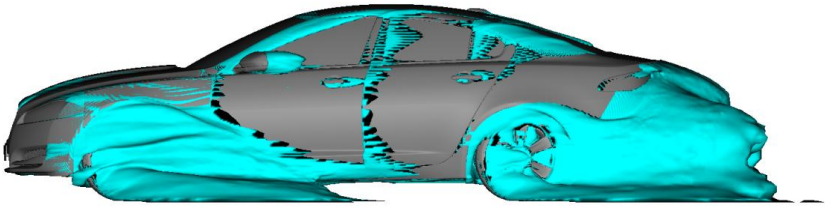

Figure 5-7 Isosurface representing $C_{p_{tot}}$ values equal to or lower than 0 for XF Saloon Case 1 – Without MVG&RW

The formation of wheel wakes is a well-known phenomenon and has been shown to contain different pairs of vortices (Wäschle, 2007). The vortices in Figure 5-8 corresponds to those described by Wäschle, except for one which originates from the front "mudflap" of the XF. When MVG&RW conditions are applied, a horseshoe formed vortex is formed around the lower part of the wheel (vortex number 2 in Figure 5-8). This vortex is present in the all stationary Case 1 as well, seen as vortex 2 in Figure 5-9, and is weakened and stretched out when wheel rotation is applied. Wäschle also described how a horseshoe formed rim vortex in formed, seen as vortex 3 in both cases, due to separation on the rim. In the case of the XF, this rim vortex is disturbed and overlapped by the mudflap vortex (number 4 in Figure 5-8 and Figure 5-9). In the case of MVG&RW, yet another vortex interferes with the rim vortex. This can be seen as vortex number 5 in Figure 5-8 and is caused by air being forced forward in the wheelhouse by the wheel rotation and leaves the wheelhouse at the front of the wheel. Air is also leaving the wheelhouse as vortex number 1, which is stronger in Figure 5-9 as more air is vented from the wheelhouse here compared to Case 2. An interesting note is that even though the front end of the two models are more or less identical the vortex structure around the front wheel differers slightly, indicating that the difference in rear end flow structures influence the front end as well.

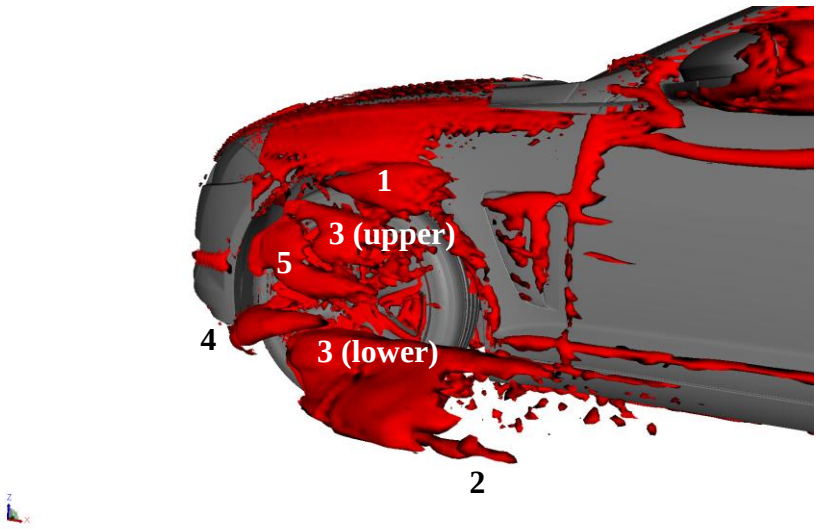

Figure 5-8 Isosurfaces of Q greater than 3000 for XF Saloon Case 2 FW – With MVG&RW

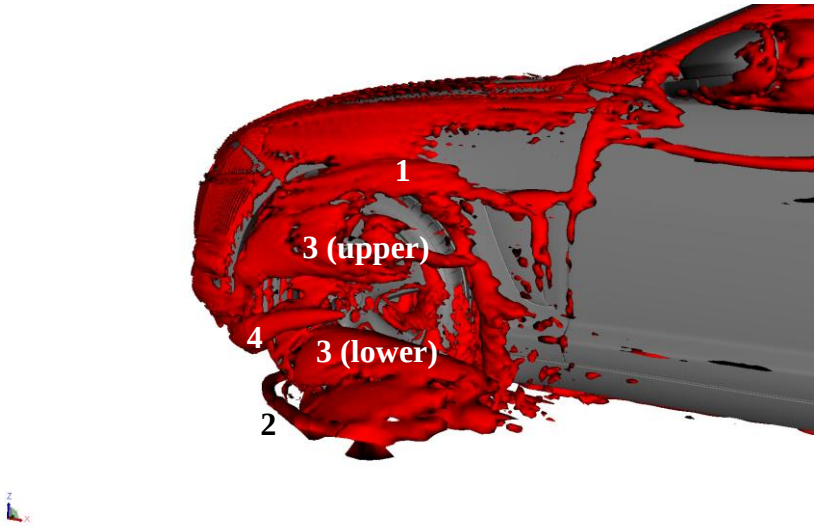

Figure 5-9 Isosurfaces of Q greater than 3000 for XF Saloon FW Case 1 – Stationary

Although not discussed by Wäschle, vortex structures are clearly visible also around the rear wheels. The difference in the vortex structures between Figure 5-11 representing the stationary Case 1 and Figure 5-10 representing Case 2 with MVG&RW, arise mostly due to rear wheel rotation, however front wheel rotation has a slight effect of fortifying the vortex named as number 3 in Figure 5-10. The addition of moving ground fortifies vortex number 2 to some degree. By comparing Figure 5-10 and Figure 5-11 it can be seen that the vortices present at number 1 becomes less and thinner with MVG&RW, permitting vortex number 2 and number 3 to grow. It can also be seen that with MVG&RW the area at number 4 fills up with vortices due to the upwash created by the rotating rear wheels. The bleeding vortex at number 5 in Figure 5-10 is only apparent in the XF Saloon and is belived to arise from interference with the C-pillar vortex.

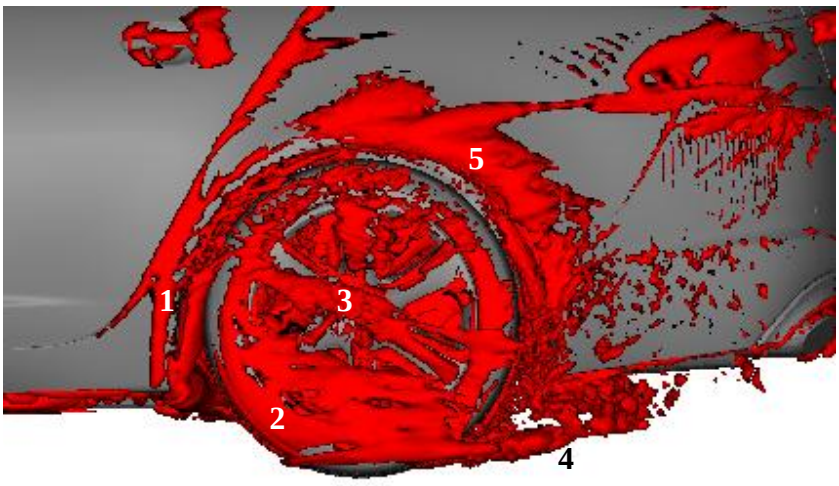

Figure 5-10 Isosurfaces of Q greater than 3000 for XF Saloon RW Case 2 – MVG&RW

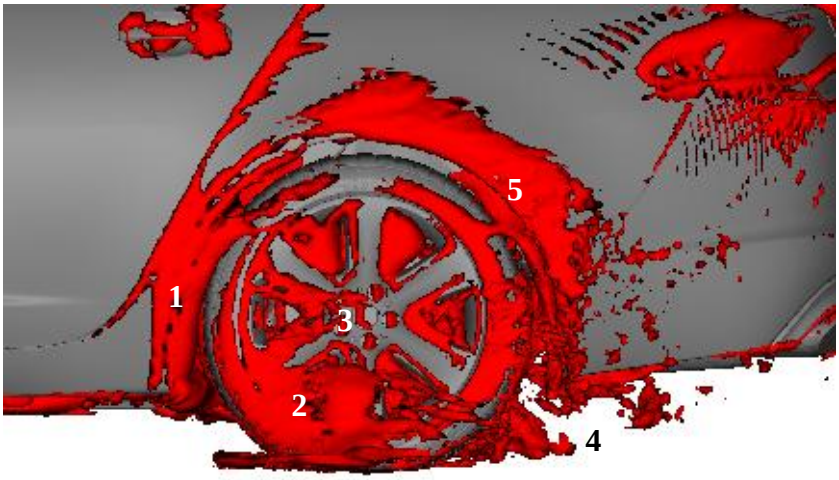

Figure 5-11 Isosurfaces of Q greater than 3000 for XF Saloon RW Case 1 – Stationary

5.2 Effect due to moving ground

In Table 5-2 and Figure 5-12 the results due to only a moving ground are presented and compared to those of (Elofsson & Bannister, 2002) and (Wickern & Lindener, 2000). There is an increase in drag and front lift due to MVG for both the XF Saloon and the XF Sportbrake, whereas there is a decrease of rear lift, which is in accordance to the results presented by Elofsson and Bannister, and partly in accordance with Wickern and Lindener who showed a decrease in front lift as well as in rear lift for a Sportscar due to MVG. According to Elofsson and Bannister the rear lift decrease due to MVG possibly depend on increased mass flow under the rear underbody of the vehicle.

Table 5-2 Results due to the effect of MVG

Notes		ΔC_D	ΔC_{LF}	ΔC_{LR}
ELOFSSON & BANNISTER				
Volvo Generic Sedan		+0.006	+0.003	-0.009
Volvo Generic Sqrback		+0.004	+0.001	-0.011
WICKERN & LINDENER				
Sportscar		+0.008	-0.005	-0.010
JAGUAR XF SALOON				
MVG - Baseline	XF Saloon	+0.011	+0.007	-0.028
JAGUAR XF SPORTBRAKE				
MVG - Baseline	XF Sportbrake	+0.009	+0.007	-0.044

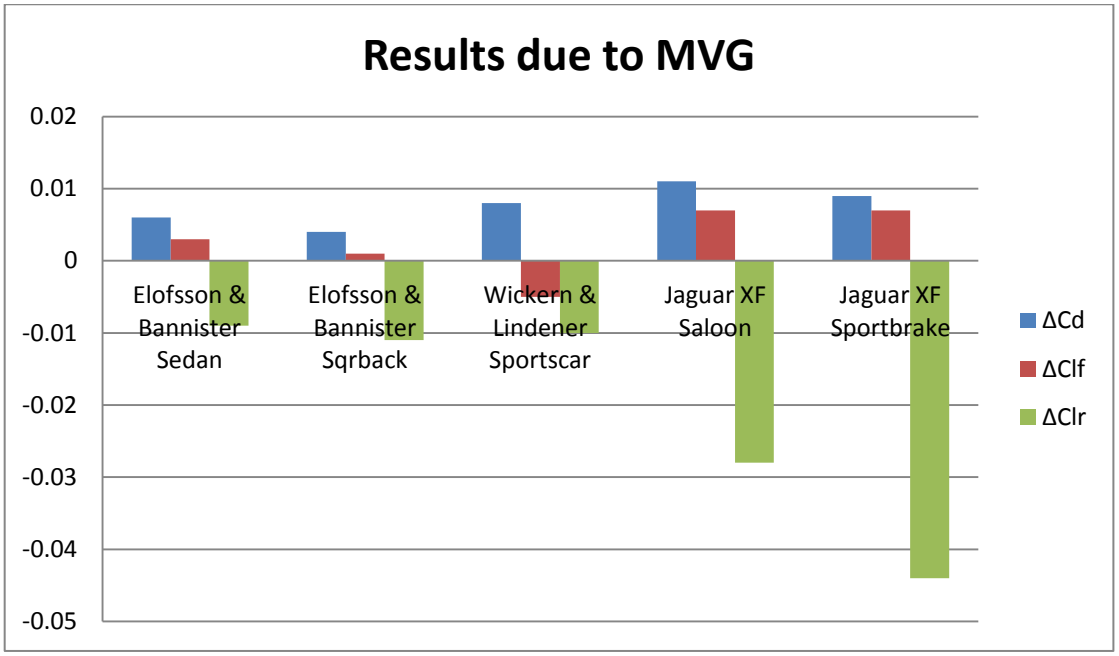

Figure 5-12 Results due to the effect of MVG

The local drag as seen on plane A4 for the XF Sportbrake can be seen in Figure 5-13 with MVG and Figure 5-14 without MVG. There is a wider high drag area starting just upstream of the rear wheels due to MVG, and also a slightly changed base wake in the sense that it is more centralised without the small wake structures as seen around the exhaust gas pipes in Figure 5-14.

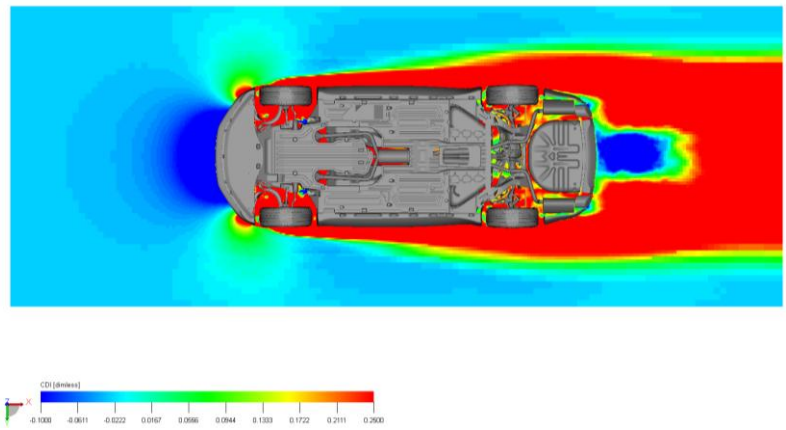

Figure 5-13 Local drag as seen on plane A4 for XF Sportbrake Case 8 – With MVG

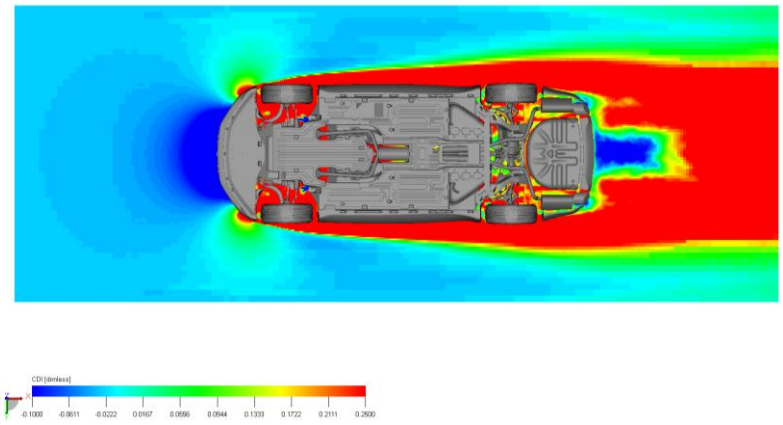

Figure 5-14 Local drag as seen on plane A4 for XF Sportbrake Case 1 – Without MVG

Figure 5-15 show the local drag as seen on plane A3 for the XF Sportbrake with MVG (Case 8), and Figure 5-16 the XF Sportbrake without MVG (Case 1), and a significant difference can be noticed due to the moving ground. There is a build-up of friction drag on the floor in Figure 5-16, which is nonexistent in the case with moving ground (Figure 5-15). The shape and size of the base wake has also changed due to the moving ground, which is more visible in Figure 5-17 and Figure 5-18, which show the pressure losses of the XF Sportbrake with MVG and without MVG respectively. Noticeable is the large effect the MVG has on the wheel and wheelhousing areas, changing the wake structures altogether. This seems to propagate down to the base wake where the wake not only changes size and shape, but also direction. With moving ground the base wake is being pulled down, which also can be seen in Figure 5-15 and Figure 5-16.

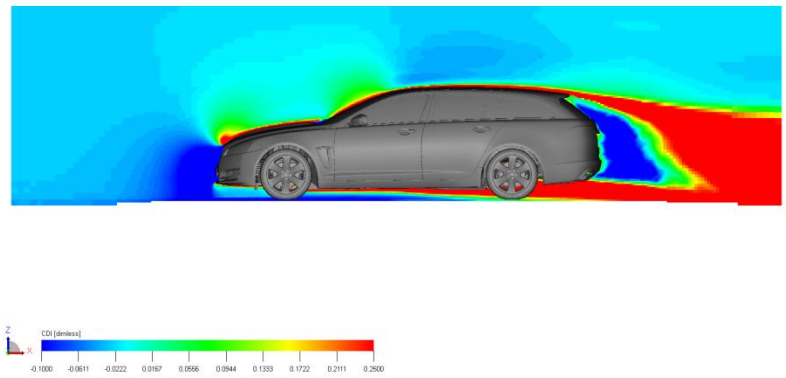

Figure 5-15 Local drag as seen on plane A3 for XF Sportbrake Case 8 – With MVG

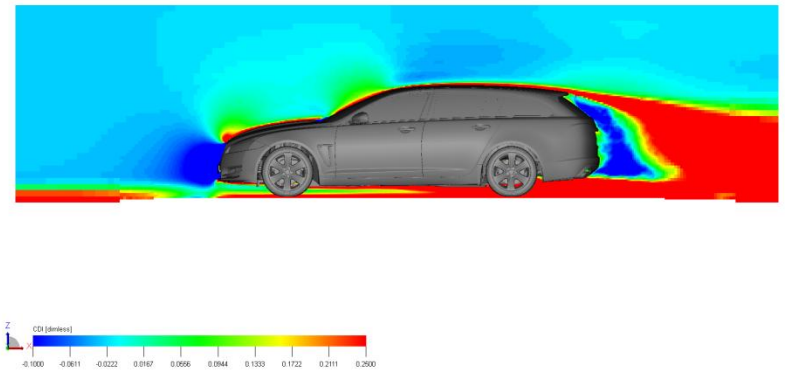

Figure 5-16 Local drag as seen on plane A3 for XF Sportbrake Case 1 – Without MVG

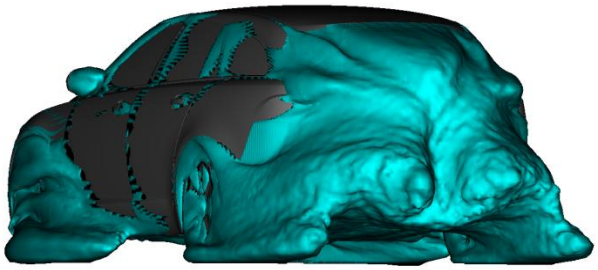

Figure 5-17 Isosurface representing $C_{p_{tot}}$ values equal to or lower than 0 for XF Sportbraken Case 8 – With MVG

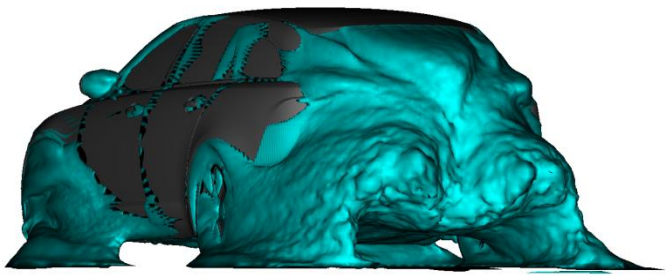

Figure 5-18 Isosurface representing $C_{p_{tot}}$ values equal to or lower than 0 for XF Sportbrake Case 1 – Without MVG

5.3 Effect due to front wheel rotation

In Table 5-3 the results due to front wheel rotation are presented and compared to those of (Elofsson & Bannister, 2002) and (Wickern & Lindener, 2000). Both results with and without MVG and rotating rear wheels are presented. Figure 5-19 graphically presents the same results due to RWF as Table 5-3 for the XF Saloon only, and Figure 5-20 for the XF Sportbrake only.

There is a very slight increase in drag for the XF Saloon due to rotating front wheels for all cases, and small changes in both front and rear lift. The cases without MVG experience a larger increase in lift values due to front wheel rotation than the cases with moving ground. When comparing Elofsson and Bannister's Volvo generic Sedan, Wickern and Lindener's Sportscar and the XF Saloon with the same conditions (with MVG and without RWR) it can be seen that there is a difference in the large increase in front lift due to front wheel rotation shown in previous result that the XF Saloon does not show.

The XF Sportbrake also experience a slight drag increase due to rotating front wheels except for the setup with a stationary ground and without rotating rear wheels. By comparing the Elofsson and Bannister Volvo generic Squareback and the XF Sportbrake with the same conditions (with MVG and without RWR) it can be noted that also for the XF Sportbrake the difference compared to earlier results lies within the front lift. The Volvo generic Squareback show an increase of 14 counts in front lift due to rotating front wheels, whereas the XF Sportbrake show a decrease of 7 counts.

Table 5-3 Results due to the effect of RWF

Notes	ΔC_D	ΔC_{LF}	ΔC_{LR}	RWR?	MVG?
ELOFSSON & BANNISTER					
Volvo Generic Sedan	-0.002	+0.017	+0.002	No	Yes
Volvo Generic Sqrback	+0.002	+0.014	-0.009	No	Yes
WICKERN & LINDENER					
Sportscar	0.000	+0.022	+0.006	No	Yes
Sportscar	-0.002	+0.018	+0.009	Yes	Yes
JAGUAR XF SALOON					
MVG&RWF – MVG	+0.003	-0.002	-0.002	No	Yes
MVG&RW – MVG&RWR	+0.003	+0.001	-0.001	Yes	Yes
RWF - Stationary	+0.002	+0.009	+0.002	No	No
RW - RWR	+0.004	+0.010	+0.002	Yes	No
JAGUAR XF SPORTBRAKE					
MVG&RWF – MVG	+0.003	-0.007	-0.001	No	Yes
MVG&RW – MVG&RWR	+0.003	-0.001	-0.004	Yes	Yes
RWF - Stationary	0.000	+0.004	-0.012	No	No
RW - RWR	+0.004	+0.008	-0.001	Yes	No

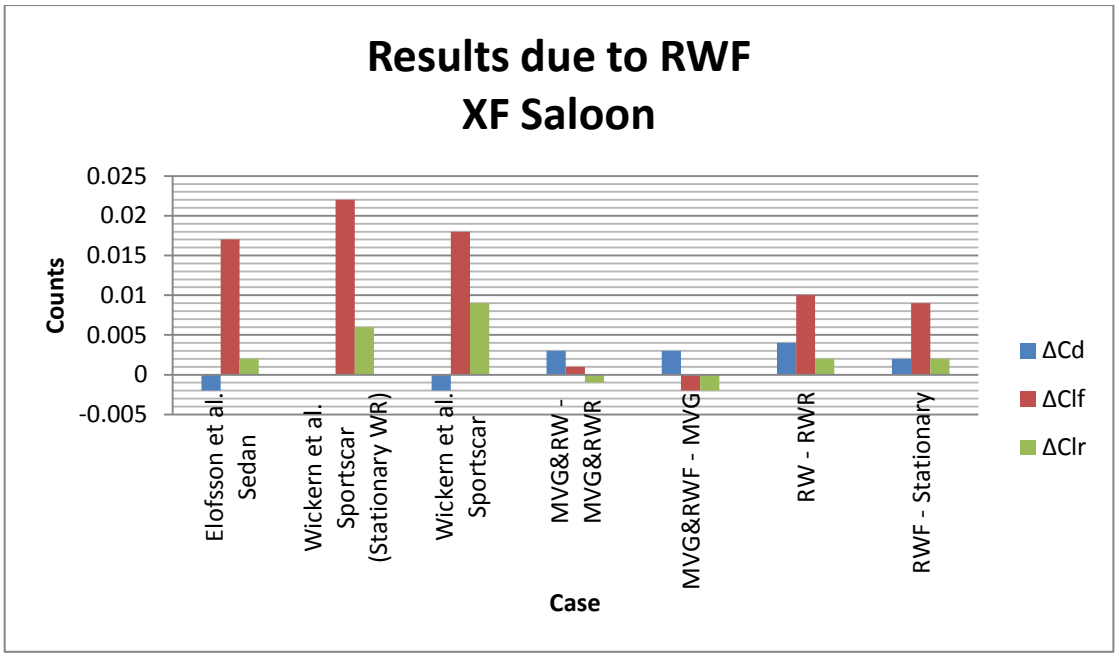

Figure 5-19 Results due to the effect of RWF - XF Saloon

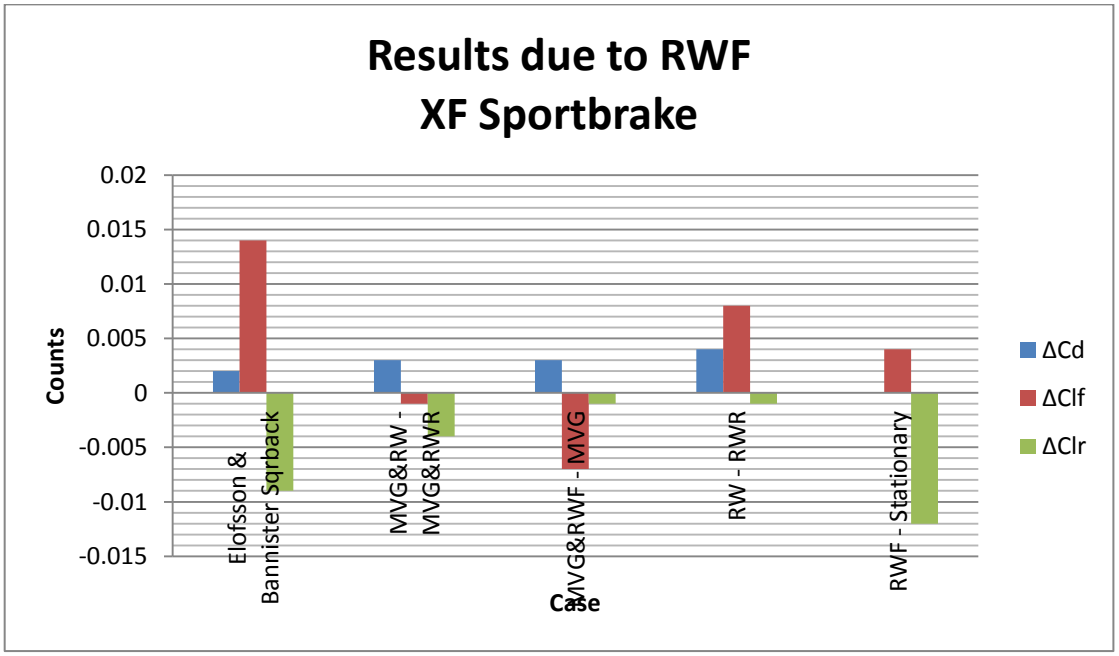

Figure 5-20 Results due to the effect of RWF - XF Sportbrake

Altogether the effects due to rotating front wheels are small in comparison to the effects due to moving ground and due to rotating rear wheels. There are however some clear trends that can be noted when comparing the cases mentioned in Table 5-3 for both the XF Saloon and the XF Sportbrake.

First, there is a local drag reduction 450 mm behind the front wheel (represented by plane B1), which can be seen by comparing Figure 5-21 which show the local drag as seen on plane B1 for XF Saloon Case 3 (with RWF) and Figure 5-22 for XF Saloon Case 8 (without RWF). Figure 5-21 shows a narrower wake behind the front wheel

due to front wheel rotation, than Figure 5-22, which is in compliance with the results presented by Elofsson and Bannister of a localised drag decrease at B1.

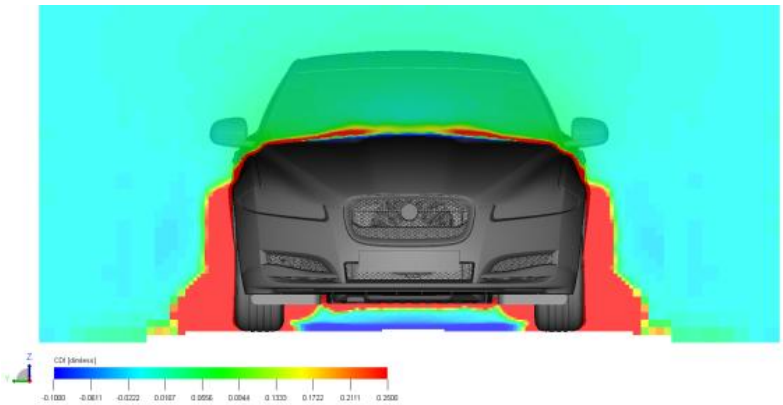

Figure 5-21 Local drag as seen on plane B1 for XF Saloon Case 3 – With RWF

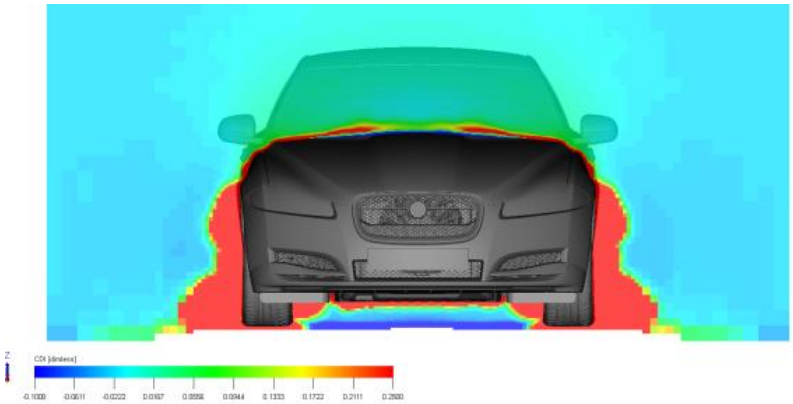

Figure 5-22 Local drag as seen on plane B1 for XF Saloon Case 8 – Without RWF

The decrease in local drag at B1 can also be noticed by comparing Figure 5-23 and Figure 5-24 which shows the vortices around the front wheels for the XF Saloon with RWF and without RWF respectively. By studying the area just behind the wheel housing in both Figure 5-23 and Figure 5-24 it is noticeable, albeit barely, that there is less vortices present locally in the area 450 mm behind the wheel centre, which represents plane B1. According to Elofsson and Bannister the local drag at the front wheel is largely dependent on vehicle configuration and wheelhouse design and can either increase or decrease due to RWF.

Secondly, there is a vortex build-up at the leading edge of the front rim due to rotation (Figure 5-23) which is not present in the cases without front wheel rotation (Figure 5-24).

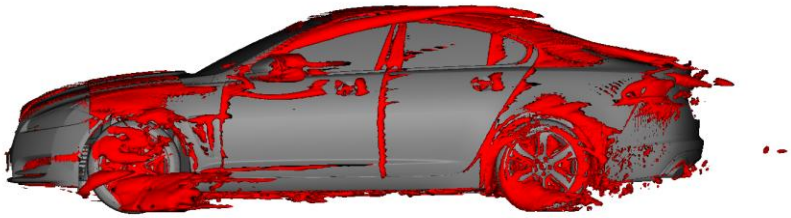

Figure 5-23 Isosurfaces of Q greater than 3000 for XF Saloon Case 3 – With RWF

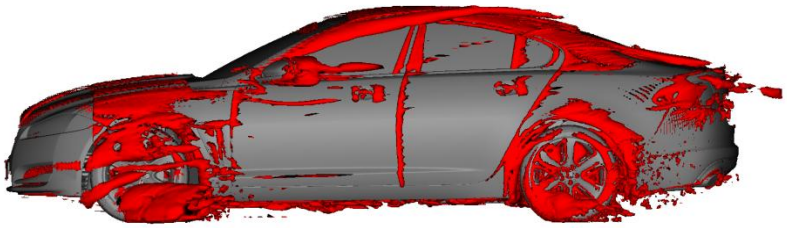

Figure 5-24 Isosurfaces of Q greater than 3000 for XF Saloon Case 8 – Without RWF

Thirdly, there is little change in the global flow field downstream of the front wheel, which can be seen by comparing the pressure losses shown in Figure 5-25 for the XF Saloon with rotating front wheels and Figure 5-26 for the XF Saloon without rotating front wheels. The rear wheel wake change very little due to front wheel rotation, even though the oncoming wake from the rotating front wheels is smaller, leaving the size of the base wake fairly unchanged as well. The only noticeable difference downstream of the front wheels due to front wheel rotation is a slight change in the shape of the pressure losses in the base wake area, to look more like the static case than the case with MVG&RW.

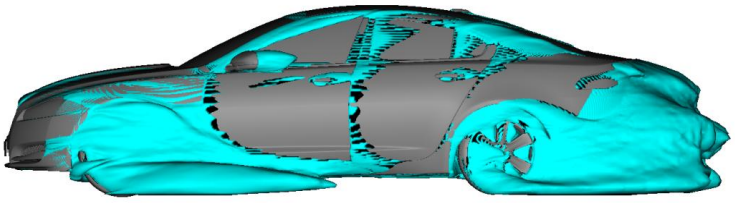

Figure 5-25 Isosurface representing $C_{p_{tot}}$ values equal to or lower than 0 for XF Saloon Case 3 – With RWF

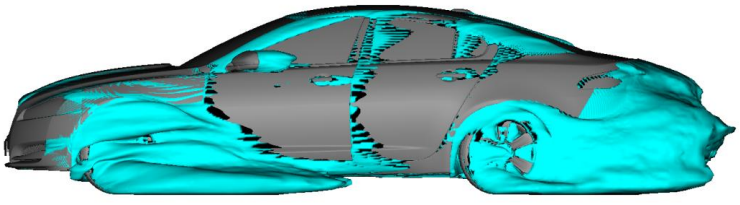

Figure 5-26 Isosurface representing $C_{p_{tot}}$ values equal to or lower than 0 for XF Saloon Case 8 – Without RWF

5.4 Effect due to rear wheel rotation

In Table 5-4 the results due to rear wheel rotation are presented and compared to those of (Elofsson & Bannister, 2002) and (Wickern & Lindener, 2000). Both results with and without MVG and rotating front wheels are presented. Figure 5-27 graphically presents the same results due to rear wheel rotation as Table 5-3 for the XF Saloon only, and Figure 5-28 for the XF Sportbrake only.

There is a significant decrease in drag and rear lift for the XF Saloon, whereas the front lift experience a slight decrease for all setups except for the one with MVG and stationary rear wheels. The decrease in drag is in line with results from both Elofsson and Bannister and Wickern and Lindener. When comparing Elofsson and Bannister's Volvo generic Sedan, Wickern and Lindener's Sportscar and the XF Saloon with the same conditions (with MVG and RWF) it can be seen that the results from the simulation show a similar trend due to rear wheel rotation, except for rear lift which decrease significantly for the XF Saloon.

The XF Sportbrake also show a large decrease in drag and rear lift, and a slight decrease in front lift due to rear wheel rotation. By comparing Elofsson and Bannister's Volvo generic Squareback and the XF Sportbrake with the same conditions (with MVG and RWF) it can be seen that the XF Sportbrake show a much larger decrease in drag and rear lift than the Squareback, which probably depend on the different rear end shape of the Volvo Generic Squareback, which is very square, and of the XF Sportbrake which is more round and tapered.

Table 5-4 Results due to the effect of RWR

Notes	ΔC_D	ΔC_{LF}	ΔC_{LR}	RWF?	MVG?
ELOFSSON & BANNISTER					
Volvo Generic Sedan	-0.019	-0.004	+0.002	Yes	Yes
Volvo Generic Sqrback	-0.008	-0.005	-0.019	Yes	Yes
WICKERN & LINDENER					
Sportscar	-0.020	-0.009	-0.002	Yes	Yes
Sportscar	-0.018	-0.005	-0.005	No	Yes
JAGUAR XF SALOON					
MVG&RW – MVG&RWF	-0.022	-0.005	-0.025	Yes	Yes
MVG&RWR – MVG	-0.022	+0.002	-0.025	No	Yes
RW – RWF	-0.021	-0.006	-0.019	Yes	No
RWR - Stationary	-0.023	-0.007	-0.019	No	No
JAGUAR XF SPORTBRAKE					
MVG&RW – MVG&RWF	-0.021	-0.003	-0.039	Yes	Yes
MVG&RWR – MVG	-0.021	-0.003	-0.036	No	Yes
RW – RWF	-0.025	-0.005	-0.024	Yes	No
RWR - Stationary	-0.028	-0.009	-0.035	No	No

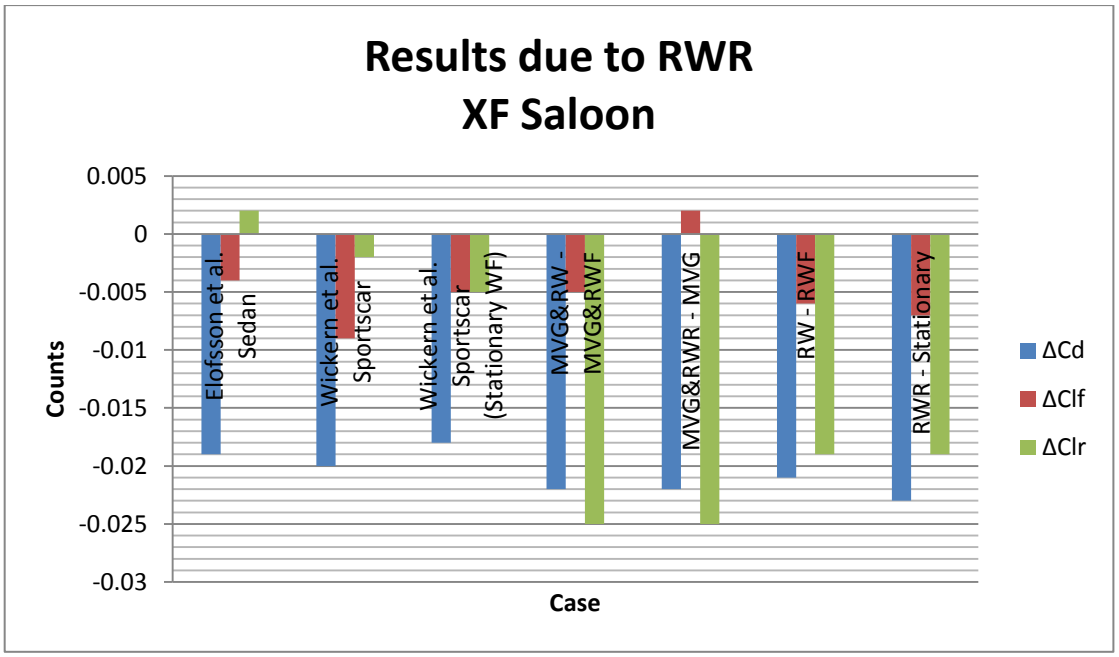

Figure 5-27 Results due to the effect of RWR - XF Saloon

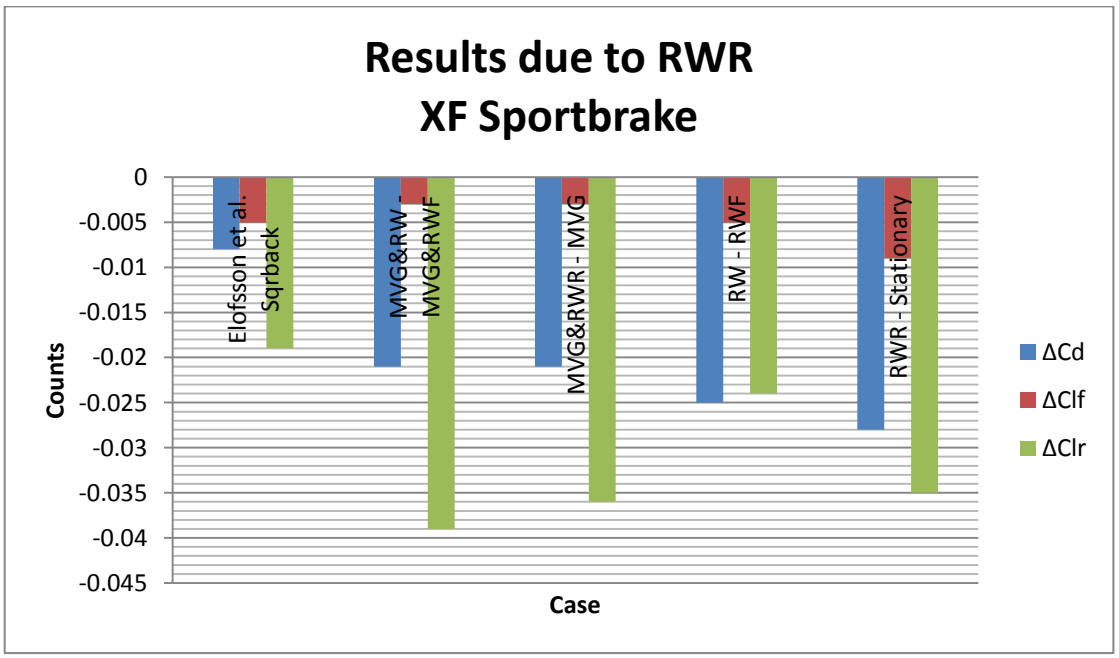

Figure 5-28 Results due to the effect of RWR - XF Sportbrake

As with the results due to RWF, the results due to rear wheel rotation also show the same tendencies for the XF Saloon and the XF Sportbrake. There is a fairly large drag decrease of about 20 counts, a minor front lift change of about 5 counts, and an increase in rear downforce of about 20 counts for the XF Saloon and about 30 counts for the XF Sportbrake.

Figure 5-29 and Figure 5-30 show the local drag 100 mm behind the vehicle (plane A1) for the XF Sportbrake with RWR and without RWR respectively. As can be seen

the dark blue area increase with RWR, indicating a local drag decrease just behind the vehicle.

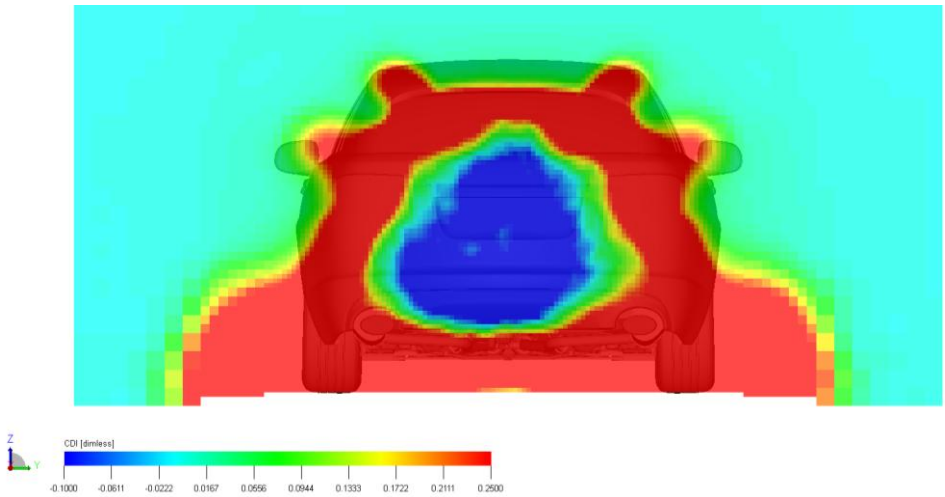

Figure 5-29 Local drag as seen on plane A1 for XF Sportbrake Case 2 – With RWR

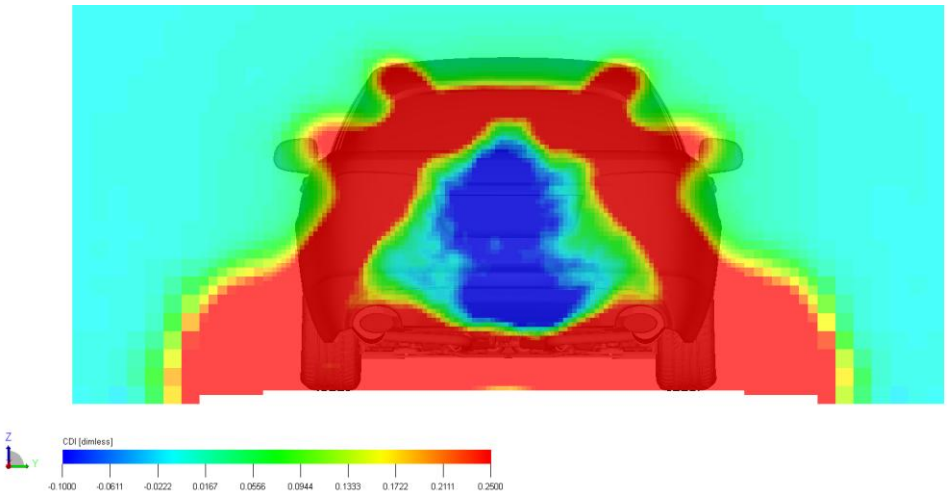

Figure 5-30 Local drag as seen on plane A1 for XF Sportbrake Case 3 – Without RWR

In Figure 5-31 it can be seen that the area just behind the rear wheels have become both shorter and narrower due to the rotating rear wheels, compared to Figure 5-32, and that it is formed as an up-wash. This area further on interacts with the base wake, changing both its size and shape, so that the centre of the wake moves upwards.

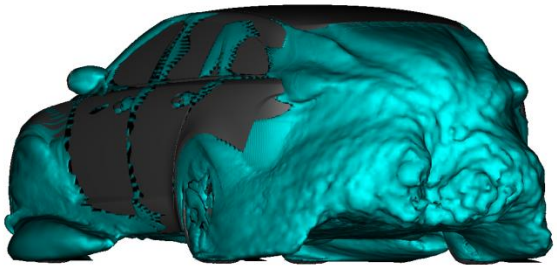

Figure 5-31 Isosurface representing $C_{p_{tot}}$ values equal to or lower than 0 for XF Sportbrake Case 2 – With RWR

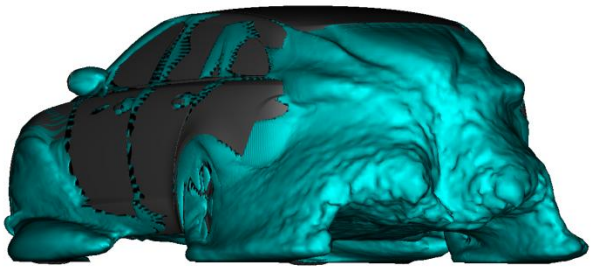

Figure 5-32 Isosurface representing $C_{p_{tot}}$ values equal to or lower than 0 for XF Sportbrake Case 3 – Without RWR

Another large change that occurs with rotating rear wheels is presented in Figure 5-33 and Figure 5-34, which show the standard deviation values of the total pressure coefficient exceeding 0.075, for the XF Sportbrake with RWR and without RWR respectively. Figure 5-33 clearly shows a significantly smaller area in the base wake than Figure 5-34, indicating that the cases with rotating wheels experience less turbulent fluctuations.

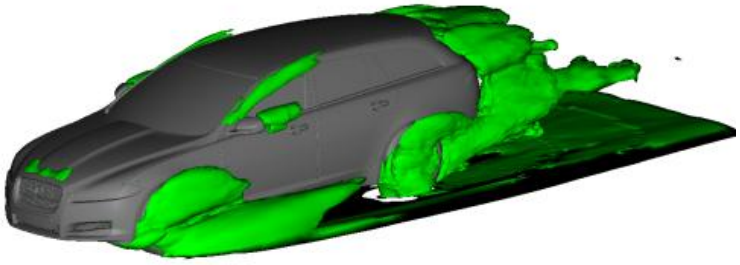

Figure 5-33 Isosurfaces representing standard deviation Cp values above 0.075 for XF Sportbrake Case 2 - With RWR

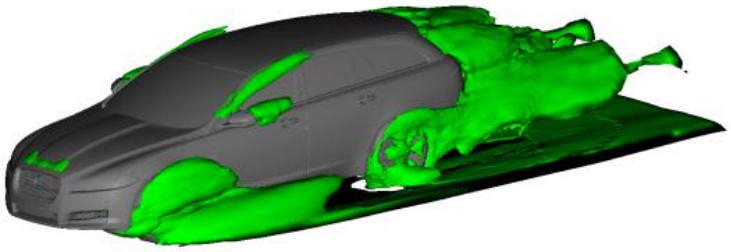

Figure 5-34 Isosurfaces representing standard deviation Cp values above 0.075 for XF Saloon Case 3 - Without RWR

5.5 Effect due to unsteadiness

When applying MVG&RW conditions additional sources of unsteadiness are introduces and the time needed to reach convergence might be prolonged. This becomes evident when comparing the required simulation time for the different cases to reach a steady behaviour. This is especially true when it comes to the XF Sportbrake which, even without rotating wheels and moving ground, represents a geometry with a large area of separated unsteady flow in the rear of the car. By comparing Case 1 and Case 2 the required simulations time for the XF Saloon increased by 73% and 64% for the XF Sportbrake. The Case 1 simulations were however seeded, and so were the Case 2 XF Sportbrake simulations as well, so the comparison is not entirely fair. The simulation times and time steps for all cases can be found in Appendix C *CPU Time (number of timesteps)*. In general it can be said that the XF Sportbrake requires, sometimes significantly, longer simulation times than the XF Saloon, even when seeded.

One way to investigate the effect that MVG&RW has on the unsteadiness of the flow is to use isosurfaces of the standard deviation of pressure. Figure 5-35 and Figure 5-36 show such isosurfaces of standard deviation ≥ 0.075 for Case 2 and Case 1 respectively on the XF Sportbrake.

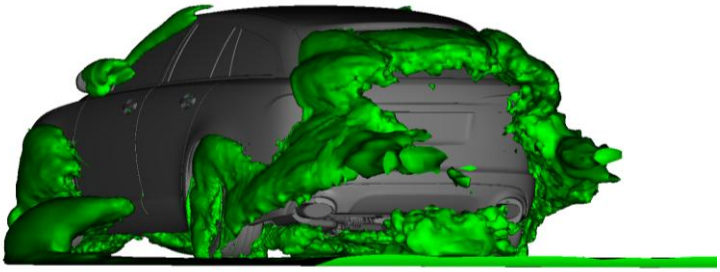

Figure 5-35 Isosurfaces representing standard deviation Cp values above 0.075 for XF Sportbrake Case 2 – With MVG&RW

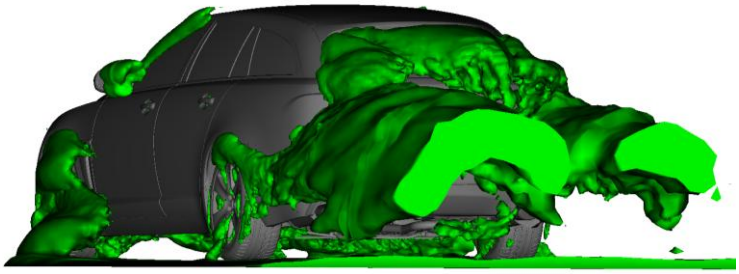

Figure 5-36 Isosurfaces representing standard deviation Cp values above 0.075 for XF Sportbrake Case 1 - Stationary

It can be seen that the wakes (indicating areas of fluctuating flow) around the wheels grows with wheel rotation while the base wake decreases in size. This is partly in contrast to what (Wäschle, 2007) suggest. He notices a smaller difference between experimental LDV and CFD data when comparing rotating wheels to stationary ones, hinting that the additional flow energy from the rotating wheels reduces the transient fluctuations. As said, the pressure standard deviation plots for Case 1 and Case 2 seems to contradict this. However when comparing the other cases, front wheel rotation and rear wheel rotation will change the shape rather than the size of the unsteady wake, and rear wheel rotation and moving ground will reduce the size of the base wake. When wheel rotation and moving ground are applied simultaneously the result is larger wheel wakes but a reduction in base wake. Further investigation shows that the differences in unsteady flow behaviour between the different cases are the same for the two models, except for the expected dissimilarities in the rear. The rear unsteady wake of the XF Sportbrake can be divided into two parts, one lower and one upper located in the backlight area just behind the D-pillars. The lower base wake more or less behaves the same as the base wake of the XF Saloon. One interesting phenomenon is the behaviour of the upper base wake. As seen in Figure 5-35 and Figure 5-36 the change in size of the lower base wake is significant while the upper base wake shows only a minor change in size. This is characteristic of the XF Sportbrake, regardless of case scenario the upper base wake is more or less consistent in shape and size. This can also be seen in Figure 5-37 and Figure 5-38, showing the pressure standard deviation on plane S1 for Case 2 and Case 3 for the XF Sportbrake. The lower base wake is increased when the rear wheel rotation is turned off in Case 3, whereas the upper base wake hardly changes at all.

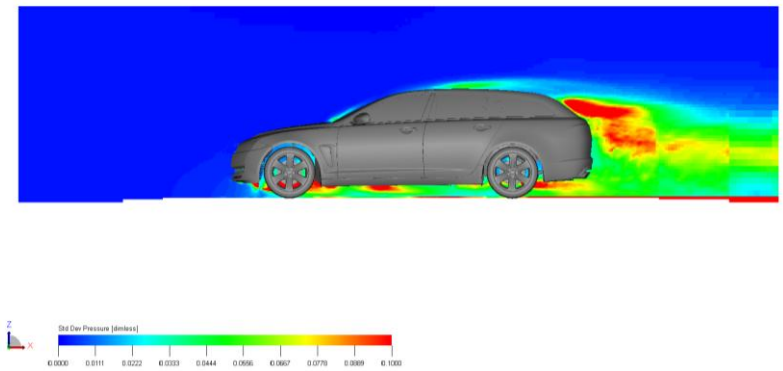

Figure 5-37 Standard deviation ≥0.075 of pressure as seen on plane S1 for XF Sportbrake Case 2 – With RWR

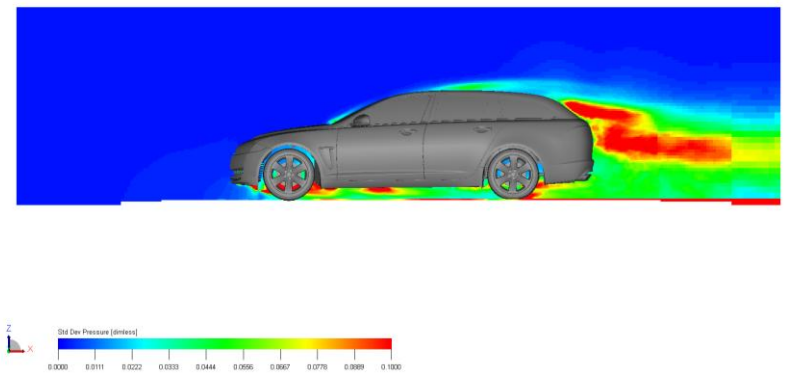

Figure 5-38 Standard deviation ≥0.075 of pressure as seen on plane S1 for XF Sportbrake Case 3 – Without RWR

A more detailed explanation can be found in Appendix D *Effect of unsteadiness (not published).*

6 Discussion

Altogether the results presented in Chapter 5 show good correlation with earlier published experimental work, however there are some discrepancies. Most obvious is the large decrease in rear lift for the XF as a result of addition of MVG and of RWR, leading to total decrease of about 50 counts for XF Saloon and about 80 counts for XF Sportbrake. It is believed that the choice of the MRF method instead of the sliding mesh method to simulate the wheel rotation contribute partly to this large decrease since it previously has been proven to create a discrepancy of about 15 counts. Further, the large difference compared to that of for example Elofsson and Bannister is also thought to be due to the design of the XF; with the XF Saloon being more similar to a Coupe than a Sedan in its design, and the XF Sportbrake having a much rounder rear end than that of Elofsson and Bannister's generic Volvo Squareback. This difference in design is also thought to be the reason why the XF Sportbrake show more significant results due to MVG&RW than the XF Saloon, compared to the results published by Elofsson and Bannister, where the Volvo generic Sedan show more significant results due to MVG&RW. Another discrepancy between the XF and earlier published results is the results due to front wheel rotation. Both the XF Saloon and the XF Sportbrake show noticeable smaller difference in front lift due to RWF than earlier result and XF Saloon also show a very small drag increase rather than a decrease due to RWF. The drag decrease should not be taken too seriously since it is very small and close to the tolerance values used to decide when the simulations are stable. No obvious reason for the lower delta values in front lift due to RWF have been found, however the changes in local drag at plane B1 appears to be less significant than those for Elofsson and Bannister.

6.1 Stationary vs. moving ground and rotating wheels

To explain the reasons of the reduction of both drag and lift when comparing Case 2 (MVG&RW) and Case 1 (Stationary) it is necessary to investigate the flow field around the vehicles for the two cases. Case 1, with its stationary conditions, is regarded as the baseline of the investigation and this configuration is still common in wind tunnel testing even though its inadequacises are well known. One of the most significant shortcomings, as described in section 3.1.4, is the formation of a boundary layer on the floor of the wind tunnel. This presence of the floor boundary layer can be seen in Figure 5-3 as the mentioned friction drag. It should be noted that skin friction drag on the floor does not add drag to the car itself, even if it might interfere with the global flow field. There is however a possibility that the floor boundary layer could affect the measured drag (and lift) values in a wind tunnel if the measuring balance is floor mounted.

The smaller base wake of Case 2 can be considered to be the most significant reason for the drag reduction when MVG&RW conditions are applied and this behaviour has aslo been previously described by (Wäschle, 2007), who explains how the rear wheel rotation puts additional energy into the wake area and thus reduces the losses and the wake size. The wake structure in Case 1 acts a nozzle hindering the underbody flow, while it more resembles a diffuser in Case 2 which increases the mass flow of air under the car and improves the pressure recovery at the rear end. This pressure recovery increases the base pressure and thus reduces the pressure drag. The increased mass flow of air under the car also explains the decrease in total lift, as the increase in

mass flow means higher air velocity which according to Bernoulli means lower pressure.

There is a negative drag propagating from the front of the vehicles which can be explained by the fact that the coefficient of total pressure can locally be greater than one, and using Equation 8 it can be seen that if the coefficient of total pressure is greater than one and the local velocities is zero (stagnation point) then the local drag is negative.

By adding up the results of the effects due to moving ground, due to front wheel rotation and due to rear wheel rotation the results end up at approximately the same values as for the cases with MVG&RW; however the results due to RWF are largely insignificant compared to the others. The increase in drag due to MVG is outweighed by the more significant decrease in drag due to RWR, adding up to an overall decrease in drag for both the XF Saloon and the XF Sportbrake of approximately ten counts. None of the results show any large change in front lift, leading to the insignificant reduction of about two counts when adding MVG&RW. Both the results due to MVG and the results due to RWR show a large decrease in rear lift adding up to the significant decrease in rear lift due to MVG&RW. This additive behaviour can also be noted when comparing ΔC_{LR} for the XF Saloon and the XF Sportbrake. The XF Saloon continuously shows a ΔC_{LR} that is 65% of that of the XF Sportbrake (except for the results due to RWF) which can be contributed to the larger area of separated unsteady flow in the rear of the XF Sportbrake as noted in section 5.5.

6.2 Effect due to moving ground

The addition of a moving ground increases both drag and front lift, whereas it decreases rear lift quite significantly. This can be explained by the removal of a boundary layer build-up on the floor, which allows for an increased airflow underneath the vehicle leading to more interaction between the wheels, the underbody and the now more energetic airflow. Again, the increased mass flow can explain the decrease in lift and might also explain the increase in drag as more air is exposed to the rough underbody.

6.3 Effect due to front wheel rotation

The addition of rotating front wheels does not have any large effect on either of the vehicles, which is interesting since earlier results indicate a rather large change in front lift due to RWF. There is however a discrepancy in the local drag decrease at plane B1 and the global drag increase due to RWF which is in compliance with Elofsson and Bannister's results, who believe it to depend on the downscaling of the front wheel wake, which then will interact less with the rear wheels and hence letting the rear wheel and wheelhousing wake grow and increase its interaction with the base wake. As can be seen when comparing Figure 5-25 and Figure 5-26 with and without front wheel rotation there is very little change around the rear wheels. However there is a very small change in pressure losses in the base wake area such that the lower part of the base wake looks more like the fully static case (Figure 5-7) than the case with MVG&RW (Figure 5-6), which can explain the increase in drag. Since the XF show the same general flow behaviour as that of previous research due to RWF, the fact that there is a discrepancy in force values due to RWF is not necessarily alarming. Elofsson and Bannister comment on this in their report as well and emphasise that the design of the vehicle and of the wheelhouse largely affect the drag around the front wheel due to RWF.

6.4 Effect due to rear wheel rotation

With a drag decrease of about 20 counts for both the XF Saloon and the XF Sportbrake, and a rear lift decrease of about 20 counts for the XF Saloon and about 30 counts for the XF Sportbrake it is evident that the addition of rotating rear wheels have a large effect on both drag and rear lift for both models.

Also earlier result have commented on the importance of RWR to the results of MVG&RW and contributed the large affect to the interaction between the local flow field around the rear wheels and wheelhousings and the base wake. This interaction can be noted when comparing Figure 5-31 and Figure 5-32, where Figure 5-31 clearly show an area of up-wash from the rotating rear wheels interacting with the base wake in an advantageous manner.

6.5 Effect due to unsteadiness

(Wäschle, 2007) suggests that the addition of flow energy due to wheel rotation reduces the transient fluctuations in the front wheel wakes, and he also uses this reasoning to explain why the base wake is reduced in size when MVG&RW conditions are applied. If this is true, that the additional flow energy reduces the wake and the unsteady behaviour then the $C_{p_{tot}}$ isosurfaces around the wheels should decrease in size due to wheel rotation. Figure 5-7 and Figure 5-6, however, show no sign of this. Figure 5-36 and Figure 5-35 rather suggest that wheel rotation increases the fluctuating behaviour in the wakes. The size and shape consistent D-pillar wake of the XF Sportbrake can then be used to explain why the simulations involving the XF Sportbrake takes longer to converge compared to XF Saloon simulations. This reasoning is however not completely consistent, since the base wake of the XF Sportbrake in Figure 5-36 (Case 1) is significantly larger than that of Figure 5-35 (Case 2), but the Case 2 simulation time is some 23 hours longer than the Case 1 simulation time. Further investigation is needed.

MVG&RW conditions increase, sometimes significantly, the required simulation time compared to stationary conditions which is seen as a fairly large negative effect of running simulations with such conditions.

7 Conclusions

The conclusions drawn from the undertaken research can be condensed into a number of points, which summarises the key findings and highlights the most important results:

- By adding MVG&RW the flow field as well as the integral force values change significantly for both the XF Saloon and the XF Sportbrake.

- The undertaken research has shown good correlation with both earlier experimental wind tunnel research and earlier CFD research. The correlation between the two car models is also good and change due to rotating wheels and moving ground is consistent.

- It has been shown that even though front wheel rotation does affect the flow, and moving ground has a large influence of the flow behaviour, the single most significant change occur when applying rear wheel rotation.

- When adding up the result of the effects due to MVG, due to RWF and due to RWR the total force values are close to those achieved by the use of MVG&RW, indicating that the effects are additive.

- By the use of a transient solver the possibility exists to investigate the fluctuating behaviour of the flow which opens up for a deeper understanding of the flow in critical areas, such as in wakes.

- The use of standard deviation as a means to understand the unsteadiness is believed to be promising, however further investigation is needed to validate the method.

- Considering that it has been shown that the required simulation time increases, sometimes significantly, when running MVG&RW simulations compared to stationary ones, the time aspect has to be taken into account when deciding between such setups.

- When using CFD for vehicle development, given the time aspect and the fact that stationary simulations generally provide good result (but not as good as with MVG&RW), it might be beneficial to initially use stationary simulations and reserve MVG&RW simulations for more detailed models later in the development process.

These conclusions are based on the Jaguar XF Saloon and XF Sportbrake which should be taken into consideration when applying them to other vehicles.

8 Recommendations

Following the undertaken research are a number of recommendations. First, considering the large influence MVG&RW have on both experimental as well as computational results the use of such conditions are recommended at least for simulations evaluating the underbody and wheel aerodynamics, however preferably for all simulations even though the increase in simulation time must be taken into consideration. Following, a couple of further studies to evaluate the influence different parameters have on the result are recommended;

- Perform further studies on the use of sliding mesh versus MRF for simulating wheel rotation.

- Evaluate the scanned tyres versus the axisymmetric tyres on the rear axle as well, since there is a more significant interaction between the rear tyres and the base wake.

- Further investigate the presence and behaviour of unsteady regions, and the usage of standard deviation as a means to identify these regions.

9 References

Bahram, K. (2008). *Comparison Between the Conventional Body-Fitted and the Lattice Boltzmann CFD Methods for the Flow around a Generic Pickup Truck.* SAE International.

Barnard, R. H. (2009). *Road Vehicle Aerodynamic Design* (Third edition ed.). St Albans: MechAero Publishing.

Boujo, E., Nakasato, K., Shiozawa, H., Miyamoto, W., Nakajima, S., & Fuse, Y. (2008). *Development of a Prediction Method for Passenger Vehicle Aerodynamic Lift using CFD.* SAE International.

Chakraborty, P., Balachandar, S., & Adrian, J. R. (2005). *On the relationship between local vortex identification schemes.* Journal of Fluid Mechanics.

Chen, S., & Doolen, G. D. (1998). *Lattice Boltzmann Method for Fluid Flows.* Annual Review of Fluid Mechanics.

Cogotti, A. (1989). *A Strategy for Optimum Surveys of Passenger-Car Flow Fields.* SAE International.

Cogotti, A. (1995). *Ground Effect Simulation for Full-Scale Cars in the Pininfarina Wind Tunnel.* SAE International.

Duncan D, B., Fischer, A., & Kandasamy, S. (2010). Validation of Lattice-Boltzmann Aerodynamics Simulation for Vehicle Lift Prediction. Montreal: ASME.

Elofsson, P., & Bannister, M. (2002). *Drag Reduction Mechanisms Due to Moving Ground and Wheel Rotation in Passenger Cars.* SAE International.

Exa Corporation. (2012). PoweCASE User's Guide - Release 4.4 Revision 2.

Fares, E. (2006). Unsteady flow simulation of the Ahmed reference body using a lattice Boltzmann approach. *Computers & Fluids, 35*, 940-950.

Fischer, O., Kuthada, T., Mercker, E., Wiedemann, J., & Duncan, B. (2010). *CFD Approach to Evaluate Wind-Tunnel and Model Setup Effects on Aerodynamic Drag and Lift for Detailed Vehicles.* SAE International.

Issa, R. (1995). *Rise of Total Pressure in Frictional Flow.* American Institute of Aeronautics and Astronautics (AIAA).

Kandasamy, S., Duncan, B., Gau, H., Maroy, F., Belanger, A., & Gruen, N. S. (2012). *Aerodynamic Performance Assessment of BMW Validation Models using Computational Fluid Dynamics.* SAE International.

Landström, C., Löfdahl, L., & Walker, T. (2009). *Detailed flow studies in clsoe proximity of rotating wheels on a passenger car.* SAE International.

McBeath, S. (2011). *Competition Car Aerodynamics* (2nd ed.). Sparkford: Haynes Publishing.

VanGordon, C. L., & Walter, J. (2008). *Overview of Wind Tunnel Testing for Automotive Development.* SAE International.

Wagner, A. J. (2008). *A Practical Introduction to the Lattice Boltzmann Method.*

Wäschle, A. (2007). *The Influence of Rotating Wheels on Vehicle Aerodynamics - Numerical and Experimental Investigations.* SAE International.

Wäschle, A., Cyr, S., Kuthada, T., & Wiedemann, J. (2004). *Flow around an Isolated Wheel - Experimental and Numerical Comparison of Two CFD Codes.* SAE International.

White, F. M. (2009). *Fluid Mechanics* (6th ed.). New York: McGraw-Hill.

Wickern, G., & Lindener, N. (2000). *The Audi Aeroacoustic Wind Tunnel: Final Design and First Operational Experience.* SAE International.

Wickern, G., Zwicker, K., & Pfadenhauer, M. (1997). *Rotating Wheels - Their Impact on Wind Tunnel Test Techniques and on Vehicle Drag Results.* SAE International.

Appendix A Sliding mesh vs. MRF (Case 2)

It has recently been shown (Kandasamy, et al., 2012) that the use of sliding mesh instead of MRF to simulate wheel rotation gives a better correlation with wind tunnel testing results, especially in terms of drag. It was also shown that the simulations with sliding mesh were consistently lower in terms of drag than the experimental values, whereas the simulations with MRF regions on the other hand were consistently higher. Generally, lift predictions were good for both methods, although a slight lift sensitivity can be noted. Between the two methods delta rear lift values of up to 13 counts are presented. It is stated that with MRF the local pressure distribution in the wheels is not as accurate as with the sliding mesh method.

In Table A-1 delta drag and lift values representing Case 2 for the XF Saloon simulated with the two different methods are presented. Noticeable is the good correlation of drag between the methods, which differs from Kandasamy et al. The pressure distribution close to the rear wheels changes considerably (Figure A-1 and Figure A-2), leading to changed interaction with the base wake, which can be seen in Figure A-3 and Figure A-4. The front wheels on the other hand are less affected by the change of simulation method. This can also be noted when studying the vortices around the front and rear wheels. In Figure A-5 and Figure A-6 it can be seen that the vortex structures around the front wheels are similar between the sliding mesh and the MRF simulations, whereas the ones around the rear wheels differ between the two methods. A noticeable vortex change can be seen on the leading lower edge of the rear wheel, where the sliding mesh simulation show several small vortices (Figure A-7) whereas in the MRF simulations they have merged together to form a large vortex (Figure A-8).

By comparing the difference between the stationary cases (Case 1) and the MVG&RW cases (Case 2) simulated with the MRF method and the sliding mesh method it can be noted that the large rear lift decrease experienced with the MRF method decrease with the sliding mesh method. As with Kandasamy et al. this difference is 13 counts. However, it is important to notice that this research does not compare the CFD results with experimental results leaving the question which of the two methods that better represents the reality of the XF open.

Table A-1 Sliding mesh versus MRF method for simulating wheel rotation

	ΔC_D	ΔC_{LF}	ΔC_{LR}
Case 2 (SM) – Case 2 (MRF)	-0.003	-0.001	+0.013

Table A-2 Comparison between Stationary (Case 1) and MVG&RW (Case 2) cases with and without sliding mesh

	ΔC_D	ΔC_{LF}	ΔC_{LR}
Case 2 (MRF) – Case 1	-0.008	-0.001	-0.055
Case 2 (SM) – Case 1	-0.011	-0.002	-0.042

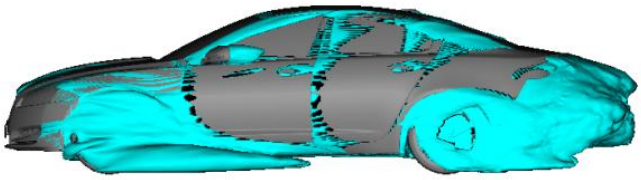

Figure A-1 Isosurfaces representing Cp values equal to or lower than 0 (Sliding Mesh)

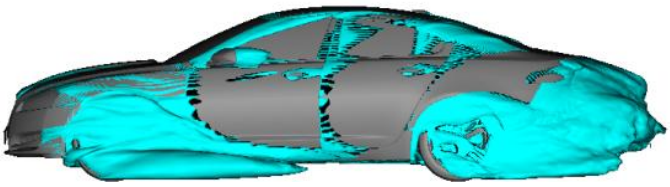

Figure A-2 Isosurfaces representing Cp values equal to or lower than 0 (MRF)

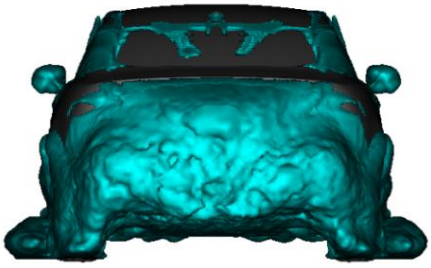

Figure A-3 Isosurfaces representing Cp values equal to or lower than 0 (Sliding Mesh)

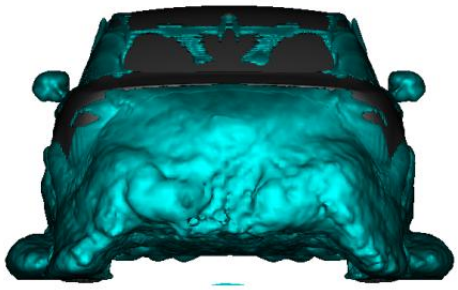

Figure A-4 Isosurfaces representing Cp values equal to or lower than 0 (MRF)

Figure A-5 Isosurfaces of Q greater than 3000 (Sliding Mesh)

Figure A-6 Isosurfaces of Q greater than 3000 (MRF)

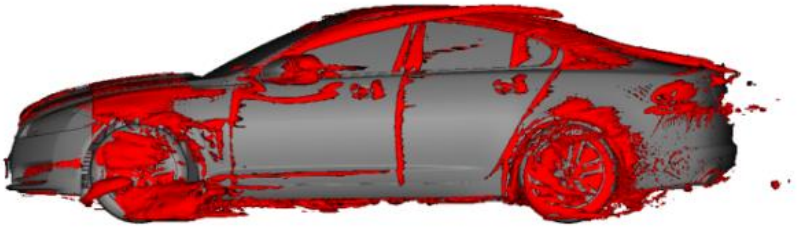

Figure A-7 Isosurfaces of Q greater than 3000 (Sliding Mesh)

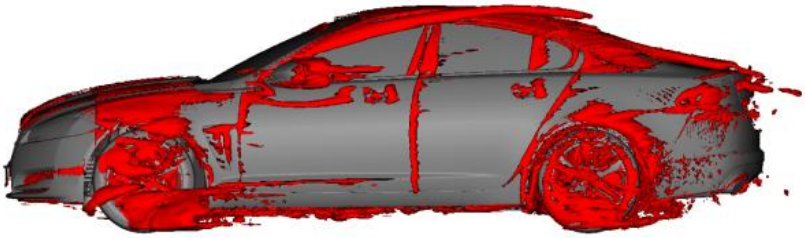

Figure A-8 Isosurfaces of Q greater than 3000 (MRF)

Appendix B Tyre Study on XF Saloon Case 4

To investigate the influence of the tyre tread and the asymmetrical shape of the scanned tyres used for static wheels, Case 4 of the XF Saloon has been simulated with both stationary scanned front tyres (Figure B-1) and with stationary axisymmetric front tyres (Figure B-2). The results can be found in Table B-1, showing a slight difference in front lift, but hardly any difference at all in drag and rear lift. Figure B-3 shows isosurfaces representing $C_{p_{tot}}$ values equal to or lower than zero for the case with scanned tyres, and Figure B-4 for the case with axisymmetric tyres, and a slight difference in the pressure field around the front wheels can be noted.

Figure B-1 Picture of a scanned tyre

Figure B-2 Picture of an axisymmetric tyre

Table B-1 Results of tyre study on Case 4 Saloon XF

	ΔC_D	ΔC_{LF}	ΔC_{LR}
Case 4 (Axisymmetric) – Case 4 (Scanned)	-0.001	+0.005	-0.001

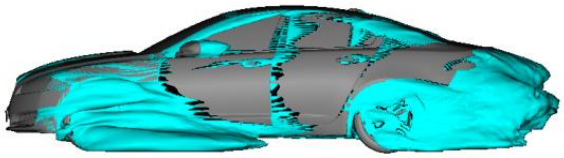

Figure B-3 Isosurfaces representing Cp values equal to or lower than 0 (Scanned tyres)

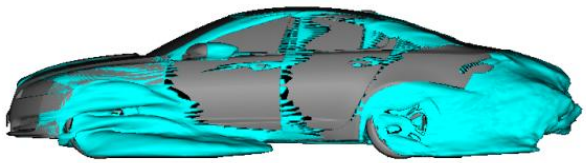

Figure B-4 Isosurfaces representing Cp values equal to or lower than 0 (Axisymmetric tyres)

Appendix C CPU Time (number of timesteps)

XF Saloon

Table C-1 CPU time and time steps for the XF Saloon

Case	Nr. of time steps	Total run time	Seeded
1	200704	37.44 hours	Yes
2	330752	64.68 hours	No
3	360448	71.51 hours	No
4	310272	60.71 hours	No
5	301056	59.83 hours	No
6	340992	67.11 hours	No
7	301056	59.47 hours	No
8	181248	27.83 hours	No

XF Sportbrake

Table C-2 CPU time and time steps for the XF Sportbrake

Case	Nr. of time steps	Total run time	Seeded
1	200704	40.99 hours	Yes
2	400000	64.3 hours	Yes
3	400000	93.4 hours	Yes
4	400000	77.11 hours	No
5	301056	71.67 hours	Yes
6	370688	59.36 hours	Yes
7	400000	80.81 hours	No
8	311296	55.26 hours	No

Appendix D Effect of unsteadiness (not published)

Appendix E XF Saloon results (not published)

Appendix F XF Sportbrake results (not published)